Máster Universitario en Ingeniería de Sistemas y de Control

Trabajo Fin de Máster

The Inverted Pendulum: Control and Sampling Strategies

Realizado por:

Ernesto Aranda Escolástico

Bajo la dirección de:

Dra. María Guinaldo Losada

Dr. Sebastián Dormido Bencomo

Junio de 2014

Curso Académico: 2013-2014

Máster Universitario en Ingeniería de Sistemas y de Control

Trabajo Fin de Máster

The Inverted Pendulum: Control and Sampling Strategies

Proyecto Tipo A: Proyecto específico propuesto por el profesor

Realizado por:

Ernesto Aranda Escolástico

Bajo la dirección de:

Dra. María Guinaldo Losada

Dr. Sebastián Dormido Bencomo

Autorización

Autorizamos a la Universidad Complutense y a la UNED a difundir y utilizar con fines académicos, no comerciales y mencionando expresamente a sus autores, tanto la memoria de este Trabajo Fin de Máster, como el código, la documentación y/o el prototipo desarrollado.

Firmado: Ernesto Aranda Escolástico

Abstract

In this master thesis, a study of the control and sampling of the inverted pendulum is presented. The modelling of the rotary inverted pendulum and the double rotary inverted pendulum are developed.

For the rotary inverted pendulum, the control strategy is divided in two parts: the swing-up control based on energy allows to reach positions close to the unstable equilibrium point. Then, three different strategies have been designed and tested for the stabilization: Full State Feedback (FSF), Linear Quadratic Regulator (LQR) and LQR based on a fuzzy model. The last design consists specifically of a Takagi-Sugeno fuzzy model to approximate the non-linear system to a succession of points where a linear system is described. A feedback gain is obtained that allows the stabilization of the inverted pendulum in a largest region of attraction than in the case of the analytic controllers. For the double rotary inverted pendulum, a LQR control is designed.

A formalism for the study of the stability of the inverted pendulum under the event-triggered control and the periodic event-triggered control is proposed. An example which shows the improvement respect to the classical time-driven control is presented. This formalism is applied to the rotary inverted pendulum.

The control and sampling strategies have been implemented in simulation and in the experimental plant. A reduction of the number of control task updates has been obtained. Moreover, we have confirmed that the fuzzy control presents the largest region of attraction.

A simulator has been deployed using Easy Java/Javascript Simulations to have a visual representation of the plants. The simulator serves as a testing ground before to the implementation of new controllers and also for educational purpose.

Key words

Inverted pendulum, modelling, control strategies, sampling, event-based control, Lyapunov stability, simulator.

Resumen

En este trabajo fin de master, se ha presentado un estudio de las estrategias de control y muestreo del péndulo invertido. Se ha desarrollado un modelo tanto del péndulo invertido rotatorio como del doble péndulo invertido rotatorio.

Para el péndulo invertido rotatorio, la estrategia de control está dividida en dos partes: el control de "swing-up" basado en energía permite alcanzar posiciones cercanas al punto de equilibrio inestable. Seguidamente, se han diseñado y probado tres estrategias diferentes para la estabilización: Realimentación total de estados, diseño óptimo LQR y LQR basado en lógica borrosa. Concretamente, el último diseño consiste en un modelo de Takagi-Sugeno para aproximar el modelo no lineal a una sucesión de puntos en los que se describe un modelo lineal. Se ha obtenido una ganancia que permite estabilizar el péndulo invertido con mayor región de atracción que en el caso de los otros dos controladores implementados, realimentación total de estados y diseño óptimo LQR. Para el caso del doble péndulo invertido rotatorio se ha diseñado un controlador LQR.

Se ha propuesto un formalismo para estudiar la estabilidad de un sistema bajo control basado en eventos y control periódico basado en eventos. Se muestra además un ejemplo en el que se observa la mejora que suponen respecto al control clásico basado en el tiempo. Este formalismo es aplicado al péndulo invertido rotatorio.

Las estrategias de control y muestreo se han implementado en la planta experimental reduciéndose el número de actualizaciones de la señal de control y confirmando que el control borroso presenta la mayor región de atracción.

Se ha desarrollado un simulador utilizado Easy Java/Javascript Simulations. El simulador sirve como banco de pruebas antes de implementar los controladores en la planta real, y también como herramienta educativa.

Palabras clave

Péndulo invertido, modelado, estrategias de control, muestreo, control basado en eventos, estabilidad de Lyapunov, simulador.

Contents

List of Tables

List of Figures

List of Abbreviations

DRIP	Double Rotary Inverted Pendulum
EBC	Event Based Control
EjsS	Easy Java/Javascript Simulations
ETC	Event-Triggered Control
FSF	Full State Feedback
LMI	Linear Matrix Inequality
LQR	Linear Quadratic Regulator
MAC	Minimum Attention Control
NCS	Networked Control System
PETC	Periodic Event-Triggered Control
PID	Proportional Integral Derivative
RIP	Rotary Inverted Pendulum
TDC	Time-Driven Control
TS	Takagi-Sugeno

Notation

$\dot{x}$	Derivative of x with respect to time
$\|x\|$	Euclidean norm of the vector x
$\max(x)$ / $\min(x)$	Maximum/minimum value of x
$sign(x)$	A function which results $+1$ if $x > 0$ and -1 if $x < 0$
$\dot{x} = Ax + Bu$	Linear system in state space representation
A^T	Transpose of the matrix A
$\tilde{A}$	Transpose companion matrix of A
A^{-1}	Inverse of the square matrix A
I	Identity matrix
$A > B$	$A - B > 0$, i.e, $A - B$ is positive definite

List of Symbols

Symbol	Description	Value [Units]
α	Angle of the pendulum respect to the vertical axis from upright	[rad]
α'	Angle of the pendulum respect to the vertical axis from downright	[rad]
B_l	Load shaft viscous damping coefficient	[N·m·rad^{-1}]
B_m	Motor shaft viscous damping coefficient	[N·m·rad^{-1}]
B_p	Pendulum viscous damping coefficient	0.0024 [N·m·rad^{-1}]
B_r	Rotary arm viscous damping coefficient	0.0024 [N·m·rad^{-1}]
B_s	Short pendulum viscous damping coefficient	0.0024 [N·m·rad^{-1}]
ζ	Damping ratio	0.7
$\delta(t)$	Continuous delay	[s]
$e(t)$	Error between the current state and the state in the last update	
E	Energy	[J]
E_{ref}	Reference energy	0.42 [J]
η_g	Gearbox efficiency	0.90
η_m	Motor efficiency	0.69
g	Gravitational acceleration	9.81 [m·s^{-2}]
γ	Angle of the second pendulum respect to the vertical axis from upright	[rad]
h	Sampling period	[s]
I_m	Motor current	[A]
J	Cost function in LQR	
J_l	Load shaft moment of inertia	1.03·10^{-4} [kg·m^2]

J_m	Motor shaft moment of inertia	$4.61 \cdot 10^{-7}$ [kg·m^2]
J_p	Pendulum moment of inertia about its center of mass	0.0012 [kg·m^2]
J_r	Rotary arm moment of inertia about its rotation axis	0.0020 [kg·m^2]
J_s	Short pendulum moment of inertia about center of mass	$3.20 \cdot 10^{-4}$ [kg·m^2]
k_m	Motor back-emf constant	$7.68 \cdot 10^{-3}$
k_t	Motor current-torque constant	$7.68 \cdot 10^{-3}$
K	Feedback gain	
K_g	High-gear total gear ratio	70
l_p	Length of pendulum to its center of mass	0.156 [m]
l_s	Length of short pendulum to its center of mass	0.163 [m]
$\mathcal{L}$	Lagrangian	[J]
L_m	Motor inductance	$0.18 \cdot 10^{-3}$[H]
L_p	Total length of pendulum	0.337 [m]
L_r	Total length of rotary arm	0.216 [m]
L_s	Total length of short pendulum	0.200 [m]
m_h	Mass of the hinge between pendulums	0.141 [kg]
m_p	Mass of pendulum	0.127 [kg]
m_r	Mass of rotary arm	0.257 [kg]
m_s	Mass of short pendulum	0.097 [kg]
q_i	Generalized coordinate	
Q	State weight matrix in LQR	
Q_i	Non-conservative force	
R	Input weight matrix in LQR	

R_m	Motor armature resistance	2.6 [Ω]
σ	Parameter used in event-triggering condition	
t	Time	[s]
τ	Torque applied at the rotary arm	[N·m]
τ_l	Torque applied to the load shaft	[N·m]
τ_m	Torque applied to the motor shaft	[N·m]
θ	Angle of the rotary arm respect to the X axis	[rad]
θ_l	Angle of the load shaft	[rad]
θ_m	Angle of the motor shaft	[rad]
T	Controllability matrix	
$\mathcal{T}$	Kinetic energy	[J]
u	Input signal	
u_d	Delayed input signal	
$\boldsymbol{v}$	Vector of linear velocity	
V	Lyapunov function	
$\mathcal{V}$	Potential energy	[J]
V_m	Motor voltage	[V]
ω	Angular velocity	[rad·s^{-1}]
ω_n	Natural frequency of the RIP	4 [rad·s^{-1}]
$\boldsymbol{x} = (x \quad y \quad z)$	Vector of Cartesian coordinates	

1. INTRODUCTION

1.1 Problem Statement

The control of the inverted pendulum and, in particular, of the Furuta pendulum, which was proposed in [1], has been studied by many authors, (see for instance [2], [3], [4], to cite a few) and it is a common example in Control Theory. The main characteristics that make it an interesting case of study are that it is a strongly nonlinear, unstable, non minimum-phase, which affects stability margins and robustness, and underactuated system (there is only one actuator for more degrees of freedom) and, therefore, a difficult and complex system to be controlled that has been used as a benchmark to compare different control strategies.

The inverted pendulum has two equilibrium points, one of which is stable while the other is unstable. On the one hand, the stable equilibrium point corresponds to a state in which the pendulum is pointing downwards. In the absence of any control force, the system will naturally return to this state. On the other hand, the unstable equilibrium point is upwards. The different control strategies try to reach and maintain this unstable equilibrium position.

Commonly, the control strategy of the inverted pendulum is divided in two steps. First, the pendulum is balanced to its upright position. The control law for that is based on using an energy function as in [2]. Once the system is close to the unstable equilibrium point, the second step consists of applying a feedback control law, since the system can be approximated by a linear model in that case [5].

The characteristics and challenges describe above make the inverted pendulum an interesting and adequate application example to be used with master students. In the lab, students face problems which were unnoticed during the theoretical lectures, and the learning process is clearly enriched. In this regard, distance education universities as UNED have successfully addressed the problem of the widespreadness of students replacing the traditional hands-on laboratories with web-based labs [6], which should consist of a virtual and a remote counterparts. The remote lab implies that the student interacts with the real plant through the internet, sending commands and receiving

feedback from the received signals and a video streaming to and from the network, respectively.

However, the use of communication networks has brought some problems as the limited bandwidth or delays in the transmission of information. These phenomena can negatively affect the control performance, and even make unstable a closed loop system that is stable in absence of the network. Moreover, systems with fast and/or unstable dynamics, as the inverted pendulum, are more vulnerable to these network effects.

In this sense, the traditional control, in which the control signal is updated periodically (time-driven control systems), may produce an unnecessary waste of resources, as in many situations more information than the required by the plant is sent. For this reason, in recent years, the interest in the event-based control (EBC) has grown up significantly. In EBC, the control is only executed when a certain condition is violated [7]. We can say that there is an adaptation to the needs of the plant, and therefore, the event-triggered control (ETC) allows a more efficient usage of the scarce communication resources [8], [9].

In the Figure 1.1, the difference between the time based control (in blue) and the event based control (red) is shown. In the first case, the signal is sampled with a period h, whereas in the second is sampled when the signal crosses the different levels defined by δ. In this way, the number of control tasks can be reduced.

However, a new problem arises. The monitoring of the event-triggering condition causes a waste of computation resources because the condition is evaluated continuously. A possible solution is then to check the triggering condition only at prefixed instances of time. This is the idea of the periodic event-triggered control (PETC) [10]). The main difference with the conventional ETC is, therefore, that the event-triggering condition is only periodically verified; hence, the waste of the resources employed in the monitoring is reduced. In the Figure 1.2, the signal is continuously sampled in the case of the ETC. However, in the case of PETC, it is sampled only at period h, but the performance is the same.

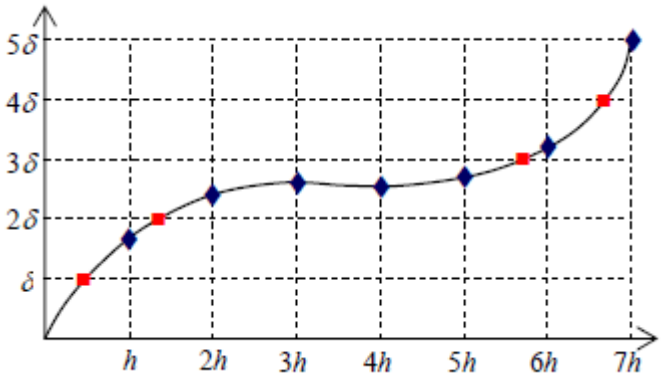

Figure 1.1: Sampling based on time (blue) and on events (red). Figure from [11]

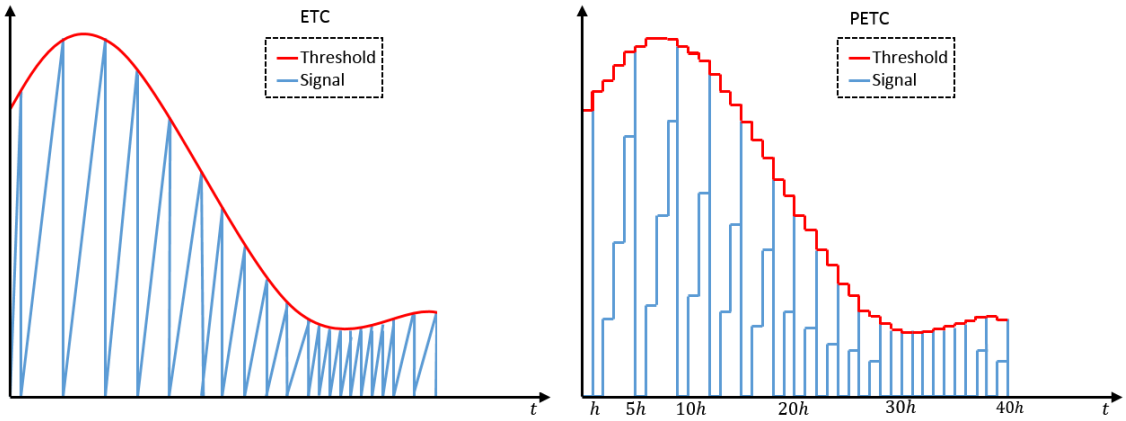

Figure 1.2: Example of ETC (left) and PETC (right)

1.2 State of Art

On one hand, the inverted pendulum is one of the most popular benchmark in problems of Control Theory. Many solutions has been proposed for the swing-up and the stabilization of the inverted pendulum in all of its different types. This is due to the fact that the inverted pendulum is a great testing ground for a lot of control algorithms in different research areas, like intelligent control or nonlinear control. Artificial neural networks has been used for the swing-up [12] and stabilization [13], [14]. Fuzzy models have been also developed [15], [16]. In addition, it has been used to test optimal control algorithms [17] and genetic algorithms [18]. Naturally, it has illustrated all kind of nonlinear techniques like partial feedback linearization [19], energy based control [20] or sliding mode control [21]. Its two noticeable inherent problems, the swing-up control and the stabilization control, have been as well attacked by PID adaptive control [22], feed-forward control [23], hybrid control [4], predictive control [24], etc. A

complete review can be found in the following surveys: In [25], more than 150 references are included since the beginnings of the studies in the 60s until the publication date in 2013. In [26], several references related with nonlinear control are presented, and intelligent control techniques can be found in [27].

On the other hand, the idea of sampling based on events appears in the last 50s when [28] introduces a method to transmit data only if there is a significant change in the signal. More recently, the first works where EBC is implemented are presented, for example, a simple example of event-based PID control can be found in [29] and a level-crossing control is used in [30]. However the real impulse of EBC came out few years later when the advantages of its application to networked control systems were realized. In these systems, the EBC has become very useful getting, for example, more efficient use of the bandwidth than the periodic control.

A networked control system (NCS) is a digital control system whose components are spatially distributed. Despite all its benefits, some undesirable phenomena have been identified such as time delays in the information transmission, randomly occurring dropped packets, quantization in the transmitted signals, etc. Therefore, some effort should be put to reduce the adverse influences of the network. In [31], [32], preliminary results of an event-triggering scheme, where the exponential stability of the resulting sampled-data system is ensured, are presented. In [33], a schedule called fixed threshold strategy has been proposed to guarantee the bounded-input bounded-output stability of the controlled system.

To deal with event-based control strategies for linear NCS, several different approaches have been proposed [9], [10], [34], [35] and also for nonlinear systems [36]. Other works propose a delay system method to investigate the NCSs under the event-based scheme [37], [38].

As far as the way the events are triggered, many papers have been published as we will detail in Section 4.3. Some of most common approaches are, for example, deadband control [39], error bounded by the state [9], based on Lyapunov functions [40] or the proposed by [41].

However, as we have mentioned, the ETC implies that the state has to be measured continuously to compute the triggering condition. To avoid this, new strategies appear such as the self-triggering [42], [41] have come up. Self-triggering computes the time t_{k+1} for the next execution from the current state x_k. The principal and inherent problem of the self-triggering is the robustness against disturbances and model uncertainties [7]. The state x_k is sampled at instances of time t_k. This measurement is used to compute the control signal, estimate future states of the system, and predict the next sampling time t_{k+1}. If the system was affected by any disturbance in the interval (t_k, t_{k+1}), the system would not be aware of it until t_{k+1}. Hence, self-triggered control is more vulnerable to disturbances.

There exists also the so called Minimum Attention Control (MAC) [43], [44], which maximize the next execution time, while a certain level of performance holds, and the Anytime Attention Control (AAC), which assumes that the signal control cannot be recomputed after each control task execution. Nevertheless, they both present similar problems of robustness to face delays and disturbances.

A complete survey of event-based control can be found in [7], which gives a whole study about EBC in NCSs and how the communication and actuation waste can be reduced. In [45], a recent review about EBC and a summary of the most recent results in the field are given.

Nevertheless, there are very few papers which apply event-based control to the inverted pendulum [46]. In this way, this master thesis is a first approach to the control of a rotary inverted pendulum using event-based control.

1.3 Goals of the Master Thesis

In this master thesis, a review of the modelling and the control laws of the Rotary Inverted Pendulum (RIP) for the swing-up and the stabilization is presented. The stabilization of the Double Rotary Inverted Pendulum (DRIP) is also studied. We also analyse the different ways of updating the control signal. The Figure 1.3 shows the prototypes of the RIP (a) and the DRIP (b) which have been used.

These general objectives are specified in the following points:

- The comparison of the classical stabilization strategies, Full State Feedback (FSF) and Linear Quadratic Regulator (LQR) with a newer approach using a LQR based on a model of Takagi-Sugeno in order to test what strategy allows a higher region of attraction to the upright position.
- The study of different ways to update the control signal, Periodic-Driven Control, ETC and PETC.
- To derive a formalism to obtain a maximum period which guarantees the asymptotic stability of the PETC and that the event condition never is violated. Moreover, it is applied to the RIP, which is a challenging system due to its fast dynamics.
- An interactive simulator of the RIP and the DRIP developed which allows a clear visualization of the physical phenomena which involve the inverted pendulum.
- The control and sampling strategies have been implemented in the experimental plant.

Figure 1.3: a) Plant of the RIP. b) Plant of the DRIP

1.4 Organization of Master Thesis

This master thesis is organized as follows:

- **Section 2** contains the specific description of the inverted pendulum, the different types, and their utility. In this section, the dynamical models of the RIP and the DRIP are derived using Lagrangian Mechanics.
- **Section 3**: In this section, different control laws are presented. In particular, for the RIP, a classical energy based swing-up strategy and three stabilization strategies (FSF, LQR, LQR based on TS fuzzy model) for the linearized model are described. For the DRIP, a stabilization control law is also shown.
- **Section 4**: The different ways to update the control task are presented. We also propose a formalism to guarantee the stabilization of ETC and PETC system. The formalism is applied to the RIP system.
- **Section 5** briefly describes the tool Easy Java/Javascript Simulations (EjsS). Moreover, an interactive simulator of the systems developed with EjsS is presented with some examples of use.
- **Section 6**: In this section the experimental results obtained with the reals plant of the Figure 1.3 are presented.
- **Section 7**: The conclusions and the future work are given.

2. MODELLING

In this section a brief introduction of the inverted pendulums is presented. Then, the models of the RIP and the DRIP are derived. The equations of motion of both plants are obtained by Euler-Lagrange method [47], [48].

2.1 Introduction

2.1.1 The Inverted Pendulum and its different types

The inverted pendulum has been studied for decades since Stephenson [49] examined an inverted pendulum and demonstrated that it could be stabilized by applying rapid, vertical, harmonic oscillations to its base [50]. Initially, in the 60s, the problem of stabilization was solved using linear methods in a pendulum on a cart. However, when the global problem, including the swing-up, was tackled, the bounded path of the cart was identified as a limitation. For this reason, Furuta designed the rotary inverted pendulum (or Furuta pendulum) (Figure 2.1) in the 70s, which avoids this limitation. However, this new implementation has a disadvantage, since the dynamics of the system are more complicated due to new centrifugal and Coriolis forces [26].

As a result of this, a complete family of pendulums has come up adding in each step more degrees of freedom. The most common are the two aforementioned, the pendulum on a cart (Figure 2.2) and the Furuta pendulum (Figure 2.1), which have two degrees of freedom. Besides these, there are other examples such as the double pendulum or those that result from adding new degrees of freedom through more links, the pendubot, the reaction wheel pendulum or the spherical pendulum [25].

2.1.2 The Utility of the Inverted Pendulum

The inverted pendulum has been widely used, as a benchmark to test new control algorithms. However, it is not only a lab experiment, as already mentioned. The obtained knowledge from the inverted pendulum has been used in real-life applications:

- The rocket stability can be seen, partially at least, as the stability of an inverted pendulum in order to maintain the rocket vertical.

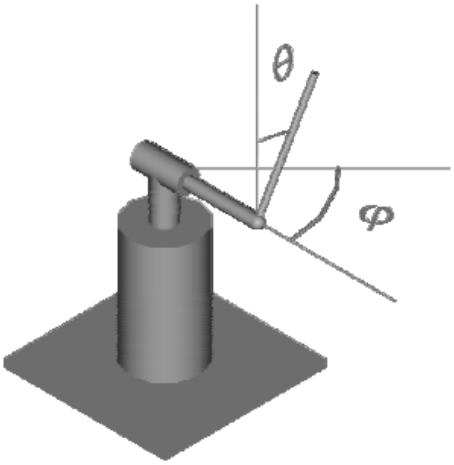

Figure 2.1: Rotary Inverted Pendulum. Figure from [51]

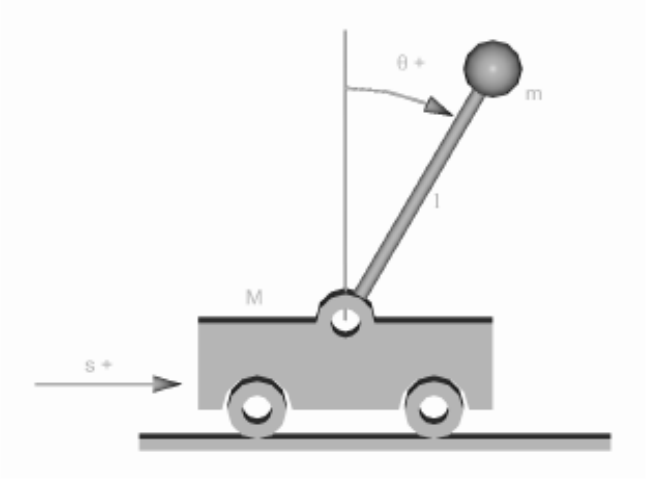

Figure 2.2: Inverted Pendulum on a cart. Figure from [51]

- The Segway personal transporter is a well-known vehicle based on the two-wheeled inverted pendulum (TWIP). The TWIP consists of a pendulum attached to a base platform that has a wheel at each side (Figure 2.3) [50].
- One important utility is the modelling the movement of robots. In order to simplify the model, many studies simulate the steps of the robot as an inverted pendulum on a cart [52].
- Related with the previous point, it can be used to study natural behaviours such as the human walking.

- The mechanism of recording earthquakes shocks of several seismometers uses an inverted pendulum [53]. It has been also utilized for the design of metronomes [54].

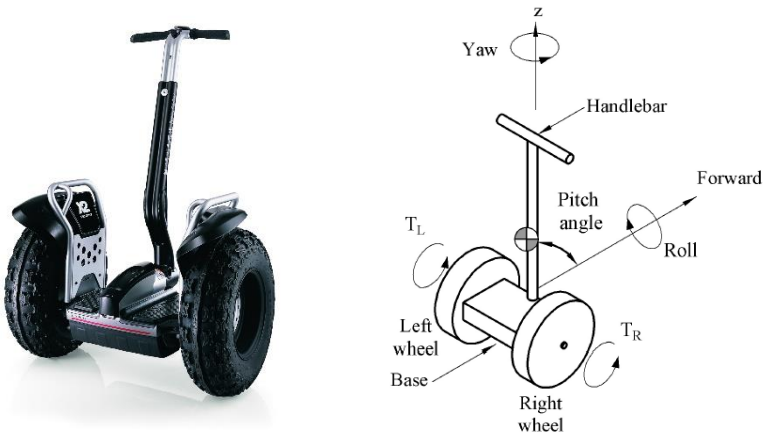

Figure 2.3: Segway transporter and diagram of two-wheeled inverted pendulum on which it is based [50]

2.2 Rotary Inverted Pendulum

The model of the rotary inverted pendulum is described in this subsection. The system is shown in Figure 2.4, where θ is the angle of the rotary arm respect to the X axis and α is the angle of the pendulum respect to the vertical axis.

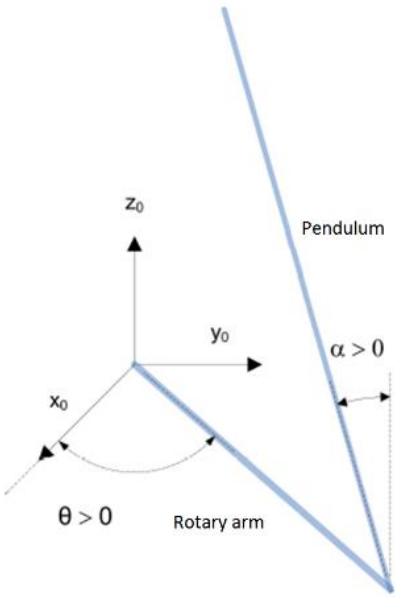

Figure 2.4: Diagram of the Rotary Inverted Pendulum

The application of Newton's laws to the RIP is not easy. Instead of that, the equations of motion of the RIP can be derived from using the Euler-Lagrange equation:

$$\frac{d}{dt}\left(\frac{\partial \mathcal{L}}{\partial \dot{q}_i}\right) - \frac{\partial \mathcal{L}}{\partial q_i} = Q_i \tag{2.1}$$

where $\mathcal{L}$ is the lagrangian, q_i are the generalized coordinates of the system and Q_i are the generalized forces, used to describe non-conservative forces. In this case:

$$(q_1 \quad q_2) = (\theta \quad \alpha)$$

$$(\dot{q}_1 \quad \dot{q}_2) = (\dot{\theta} \quad \dot{\alpha}) = \left(\frac{d\theta}{dt} \quad \frac{d\alpha}{dt}\right)$$

$$(Q_1 \quad Q_2) = \left(\tau - B_r\dot{\theta} \quad B_p\dot{\alpha}\right),$$

being τ the torque applied at the base of the rotary arm and $B_{p,r}$ the viscous damping coefficients of the pendulum and the rotary arm, respectively. The Lagrangian can be obtained from the kinetic energy ($\mathcal{T}$) and the potential energy ($\mathcal{V}$):

$$\mathcal{L} = \mathcal{T} - \mathcal{V} \tag{2.2}$$

$\mathcal{T}$ and $\mathcal{V}$ are the sum of the kinetic energy and potential energy, respectively, of all the elements of the system. They depend on the position and velocity of each element in the following way:

$$\begin{aligned} \mathcal{T}_i &= \frac{1}{2}m_i v_i^2 + \frac{1}{2}J_i\omega_i^2 \\ \mathcal{V} &= m_i g z_i, \end{aligned} \tag{2.3}$$

where i represent the i-element, m is the mass, $\boldsymbol{x} = (x \quad y \quad z)$ is the position, $v = \|\boldsymbol{v}\| = \left\|\frac{d\boldsymbol{x}}{dt}\right\|$ the linear velocity, ω the angular velocity, J is the moment of inertia respect to the center of mass, and g the gravitational acceleration. This generalization will be also useful in the case of the DRIP. For further details, see [55].

For the RIP, it is assumed that the potential energy in the rotary plane is zero and, hence, the potential energy of the rotary arm would be zero. So that the positions and the velocities are:

$$\boldsymbol{x}_r = (l_r \cos\theta \quad l_r \sin\theta \quad 0)$$

$$\boldsymbol{v}_r = (-l_r \sin\theta\, \dot{\theta} \quad l_r \cos\theta\, \dot{\theta} \quad 0)$$

$$\boldsymbol{x}_p = (L_r \cos\theta + l_p \sin\alpha \sin\theta \quad L_r \sin\theta - l_p \sin\alpha \cos\theta \quad l_p \cos\alpha)$$

$$\boldsymbol{v}_p{}^T = \begin{pmatrix} -L_r \sin\theta\, \dot{\theta} + l_p(\cos\alpha \sin\theta\, \dot{\alpha} + \sin\alpha \cos\theta\, \dot{\theta}) \\ -L_r \sin\theta\, \dot{\theta} + l_p(-\cos\alpha \cos\theta\, \dot{\alpha} + \sin\alpha \sin\theta\, \dot{\theta}) \\ -l_p \sin\alpha\, \dot{\alpha} \end{pmatrix}$$

Thus, the kinetic and potential energies are, respectively:

$$\mathcal{T} = \frac{1}{2} J_r \dot{\theta}^2 + \frac{1}{2} J_p \dot{\alpha}^2 + m_p \left(\left(L_r \dot{\theta} + l_p \cos\alpha\, \dot{\alpha} \right)^2 + \left(l_p \sin\alpha\, \dot{\alpha} \right)^2 \right)$$

$$\mathcal{V} = m_p g l_p \cos\alpha.$$

Then, from (2.1) the following two expressions are obtained:

$$\begin{aligned} &\left(m_p L_r^2 + m_p l_p^2 - m_p l_p^2 \cos^2\alpha + J_r\right)\ddot{\theta} - m_p L_p \cos\alpha\, \ddot{\alpha} \\ &\qquad + 2m_P l_p^2 \sin\alpha \cos\alpha\, \dot{\theta}\dot{\alpha} + m_p l_p L_r \sin\alpha\, \dot{\alpha}^2 = \tau - B_r \dot{\theta} \\ &-m_p l_p L_r \cos\alpha\, \ddot{\theta} + \left(J_p + m_p l_p^2\right)\ddot{\alpha} - m_p l_p^2 \sin\alpha \cos\alpha\, \dot{\theta}^2 \\ &\qquad - m_p l_p g \sin\alpha = -B_r \dot{\alpha} \end{aligned} \tag{2.4}$$

The equations (2.4) can be solved for the angles' accelerations so that

$$\begin{aligned} \ddot{\theta} &= \frac{\left[h_3 \cos\alpha \left(h_2 \cos\alpha\, \dot{\theta}^2 - B_p \dot{\alpha} + h_5 \sin\alpha\right)\right]}{H} \\ &\quad - \frac{h_4\left[\dot{\theta}(B_r + 2h_2 \dot{\alpha} \cos\alpha \sin\alpha) - \tau + h_3 \dot{\alpha}^2 \sin\alpha\right]}{H} \\ \ddot{\alpha} &= \frac{(h_2 \sin^2\alpha + h_1)\left(h_2 \cos\alpha \sin\alpha\, \dot{\theta}^2 - B_p \dot{\alpha} + h_5 \sin\alpha\right)}{H} \\ &\quad - \frac{h_3 \cos\alpha \left[\dot{\theta}(B_r + 2h_2 \dot{\alpha} \cos\alpha \sin\alpha) - \tau + h_3 \dot{\alpha}^2 \sin\alpha\right]}{H} \end{aligned} \tag{2.5}$$

where $h_1, h_2, \ldots, H$ are defined as

$$h_1 = J_r + m_p L_r^2\,, h_2 = m_p l_p^2\,, h_3 = m_p l_p L_r\,, h_4 = J_p + h_2$$

$$h_5 = m_p l_p g\,, h_6 = m_r L_r\,, H = h_1 h_4 + h_2 h_4 \sin^2\alpha - h_3^2 \cos^2\alpha.$$

Moreover, the following change of variables is made so that the number of future rules in the fuzzy control can be reduced [56]:

$$z_1 = \frac{\sin\alpha}{\alpha}\ , z_2 = \cos\alpha\ , z_3 = \dot{\theta}\cos\alpha\sin\alpha\ , z_4 = \dot{\alpha}\sin\alpha.$$

Therefore, a model of the form

$$\dot{x}(t) = A(z)x(t) + B(z)u(t)$$

is obtained, where $x^T = (\theta \quad \alpha \quad \dot{\theta} \quad \dot{\alpha})$, $z^T = (z_1 \quad z_2 \quad z_3 \quad z_4)$ and the coefficients of $A(z) = \big(a_{ij}(z)\big)$ and $B(z) = \big(b_{ij}(z)\big)$ can be derived straightforward from (2.5):

$$a_{11} = a_{12} = a_{14} = a_{21} = a_{22} = a_{23} = a_{31} = a_{41} = 0\ , a_{13} = a_{24} = 1$$

$$a_{32} = \frac{h_3 h_5 z_1 z_2}{H}\ , a_{33} = \frac{h_2 h_3 z_2 z_3 - h_4 B_r}{H}\ , a_{34} = \frac{2h_2 h_4 z_3 + h_3 z_4 - B_p}{H}$$

$$a_{42} = \frac{h_1 h_5 z_1 + h_2 h_5 (1 - z_2^2) z_1}{H}\ , a_{43} = \frac{h_2(h_2(1 - z_2^2) - h_1) - h_3 z_2 z_3 + h_3 z_4}{H}$$

$$a_{44} = \frac{(h_2(1 - z_2^2) + h_1)B_p - h_3 z_2 z_3 + h_3 z_4}{H}$$

$$b_{11} = b_{21} = 0\ , b_{31} = \frac{h_4 h_6}{H}\ , b_{41} = \frac{h_3 h_6 z_2}{H}$$

2.3 Double Rotary Inverted Pendulum

The model of the double rotary inverted pendulum is described next. Equivalent steps than for the RIP has been followed. In this case, there is a new link attached to the system (see Figure 2.5). In the design of the real plant, a shorter pendulum is placed between the rotary arm and the link of assembly of the RIP. Moreover, an encoder is collocated between both links to measure the angle of the second pendulum. Using the expressions (2.2):

$$\boldsymbol{x}_p = \begin{pmatrix} L_r\cos\theta + L_s\sin\alpha\sin\theta + l_p\sin\gamma\sin\theta \\ L_r\sin\theta - L_s\sin\alpha\cos\theta - l_p\sin\gamma\cos\theta \\ L_s\cos\alpha + l_p\sin\gamma \end{pmatrix}$$

$$\boldsymbol{v}_p{}^T = \begin{pmatrix} -L_r \sin\theta\,\dot{\theta} + L_s\big(\cos\alpha \sin\theta\,\dot{\alpha} + \sin\alpha\cos\theta\,\dot{\theta}\big) + l_p(\cos\gamma\sin\theta\,\dot{\gamma} + \sin\gamma\cos\theta\,\dot{\theta}) \\ -L_r \sin\theta\,\dot{\theta} + L_s\big(-\cos\alpha\cos\theta\,\dot{\alpha} + \sin\alpha\sin\theta\,\dot{\theta}\big) + l_p(-\cos\gamma\cos\theta\,\dot{\gamma} + \sin\gamma\sin\theta\,\dot{\theta}) \\ -L_s \sin\alpha\,\dot{\alpha} - l_p \sin\gamma\,\dot{\gamma} \end{pmatrix}$$

Then, adding its kinetic and potential energy to the obtained in the RIP and solving (2.1) for the variables $(q_1 \quad q_2 \quad q_3) = (\theta \quad \alpha \quad \gamma)$:

$$\frac{d}{dt}\left(\frac{\partial \mathcal{L}}{\partial \dot{\theta}}\right) - \frac{\partial \mathcal{L}}{\partial \theta} = \tau - B_r\dot{\theta}$$

$$\frac{d}{dt}\left(\frac{\partial \mathcal{L}}{\partial \dot{\alpha}}\right) - \frac{\partial \mathcal{L}}{\partial \alpha} = -B_s\dot{\alpha}$$

$$\frac{d}{dt}\left(\frac{\partial \mathcal{L}}{\partial \dot{\gamma}}\right) - \frac{\partial \mathcal{L}}{\partial \gamma} = -B_p\dot{\gamma}$$

the following expressions are obtained:

$$\begin{aligned} &\big[J_r L_r^2(m_s + m_p + m_h)\big]\ddot{\theta} - \big[L_r\big(m_s l_s + m_h L_s + m_p L_p\big)\cos\alpha\big]\ddot{\alpha} \\ &\quad + \big[m_p l_p L_r \cos\gamma\big]\ddot{\gamma} \\ &\quad + \big[L_r\big(m_s l_s + m_h L_s + m_p L_s\big)\sin\alpha\big]\dot{\alpha}^2 \\ &\quad + \big[m_p l_p L_r \sin\gamma\big]\dot{\gamma}^2 = \tau - B_r\dot{\theta} \end{aligned}$$

$$\begin{aligned} &-\big[L_r\big(m_s l_s + m_h L_s + m_p L_p\big)\cos\alpha\big]\ddot{\theta} + \big[J_s + m_s l_s^2 + m_h L_s^2 + m_p L_s^2\big]\ddot{\alpha} \\ &\quad + \big[m_p l_p L_s \cos(\gamma - \alpha)\big]\ddot{\gamma} - \big[m_p l_p L_s \sin(\gamma - \alpha)\big]\dot{\gamma}^2 \\ &\quad - g\big(m_s l_s + m_h L_s + m_p L_s\big)\sin\alpha = -B_s\dot{\alpha} \end{aligned} \qquad (2.6)$$

$$\begin{aligned} &-\big[m_p l_p L_r \cos\gamma\big]\ddot{\theta} + \big[m_p l_p L_s \cos(\gamma - \alpha)\big]\ddot{\alpha} + \big[J_p + m_p l_p^2\big]\ddot{\gamma} \\ &\quad + \big[m_p l_p L_s \sin(\gamma - \alpha)\big]\dot{\alpha}^2 - g m_p l_p \sin\gamma = -B_p\dot{\gamma} \end{aligned}$$

where m_s, l_s, L_s are the parameters corresponding to the new pendulum on the bottom. It is important to note the presence at a constant m_h. It represents the mass of the hinge between both pendulum and it is always oriented with α. In Section 3.2.2, a linearization of (2.6) is obtained to get a feedback gain for the stabilization of the DRIP.

Remark: Note that the torque τ is a non-conservative force, which correspond with the force that the motor should apply to the system. However, the torque cannot be applied to the plant. Instead of that, the variable which can be manipulated is the

voltage (V_m). For this reason, it is necessary to establish a relationship between the torque and the voltage. This relationship is defined as:

$$\tau = \frac{\eta_g \eta_m K_g k_t \left(V_m - K_g k_m \dot{\theta}\right)}{R_m} = m_r L_r u. \qquad (2.7)$$

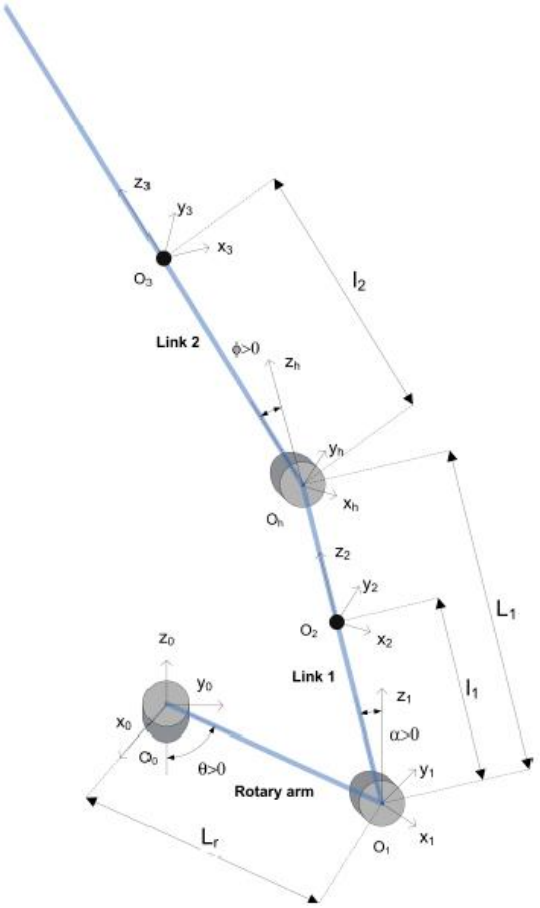

Figure 2.5: Diagram of the Double Rotary Inverted Pendulum

The parameters of (2.7) represent the gearbox efficiency (η_g), the motor efficiency (η_m), the high-gear total gear ratio (K_g), the motor current-torque constant (k_t), the motor back-emf constant (k_m), and the armature resistance (R_m), and their values can be found in the list of symbols. The derivation of this relationship can be made straightforward using the SRV-02 model of the Appendix A.

3. CONTROL LAWS

Next the swing-up control and the different control strategies for the stabilization of the rotary inverted pendulum are presented. Next, a LQR is also designed to stabilize the double rotary inverted pendulum.

3.1 Introduction

Most of the existing literature considers acceptable that two control algorithms, one to stabilize the pendulum and one for the swing-up, are required. Then, there exists a switch between the controllers at the instance of time at which the inverted pendulum can be stabilized. This occurs for the rotary inverted pendulum when α and $\dot{\alpha}$ are in the region of attraction, i.e., the range in which the stabilization controller works appropriately. Analogously, for the double pendulum, α, $\dot{\alpha}$, γ and $\dot{\gamma}$ should be inside of the region of attraction.

Many strategies have been proposed for the swing-up of the rotary inverted pendulum, for example the aforementioned [12], [21], [26]. However, in this section we use the classical energy based control, and we focus on the stabilization control in order to obtain the larger region of attraction which allows the stabilization of the pendulum. We design a LQR controller based on a fuzzy model of Takagi-Sugeno, which improves the region of attraction to the unstable equilibrium point.

3.2 Rotary Inverted Pendulum

In the case of the RIP, the control strategy is divided in two parts. The swing-up control allows to reach positions close to the unstable equilibrium point. Then, a stabilization approach yields the pendulum to the equilibria. In this master thesis, three different strategies of stabilization have been designed and tested.

3.2.1 Swing-up Control Strategy – Energy Based Control

The classical approach for the swing-up of the pendulum was developed by K. J. Åström and K. Furuta [2]. The idea is the following. First of all, let us consider the equations of motion of a single pendulum under several assumptions (no friction, the pendulum is a rigid body, and the velocity of the pivot is not limited). Moreover, instead of α, consider $\alpha' = \alpha - \pi$ in order to get the angle measured from the stable equilibrium position:

$$J_p\ddot{\alpha'} - m_p g l_p \sin\alpha' + m_p u l \cos\alpha' = 0,$$

where u is the velocity of the pivot and, in this case, the input. Let us consider the energy of uncontrolled pendulum, i.e. $u = 0$:

$$E = \frac{1}{2}J_p\dot{\alpha'^2} + m_p g l_p(cos\,\alpha' - 1).$$

It is necessary to know how the energy is affected by the acceleration of the pivot. So take the derivative of the energy with respect to time:

$$\dot{E} = J_p\dot{\alpha'}\ddot{\alpha'} - m_p g l_p \alpha'(cos\,\alpha') = -m_p u l_p \dot{\alpha'}\,cos\,\alpha'.$$

According to [2], the control of the energy is easy because the system results an integrator with varying gain. One strategy to swing-up the pendulum to a desired energy reference E_r could be a proportional control law:

$$u = \left(E - E_{ref}\right)\dot{\alpha'}\,cos\,\alpha'.$$

The goodness of the control law can be proven using the Lyapunov method [57] and taking as Lyapunov function

$$V = \frac{\left(E - E_{ref}\right)^2}{2},$$

whose derivative is:

$$\dot{V} = -m_p l\left(\left(E - E_{ref}\right)\dot{\alpha'}\,cos\,\alpha'\right)^2.$$

The Lyapunov function decreases if $\dot{\alpha}' \neq 0$ and $\cos\alpha' \neq 0$. Since the pendulum cannot maintain a stationary position with $\alpha' = \pm\pi/2$, the energy goes to E_{ref}.

Additionally, to change the energy as fast as possible the magnitude of the control signal should be as large as possible. This is achieved implementing the following control law:

$$u = \mu(E - E_{ref})sign(\dot{\alpha}' cos\,\alpha'),$$

where μ is a tunable control gain.

3.2.2 Stabilization Control Algorithms

In this subsection the stabilization control strategy is presented. The aim is to obtain a feedback gain K such that the control law is defined as:

$$u = Kx.$$

Three different strategies have been proposed to find this gain: Full State Feedback (FSF), Linear Quadratic Regulator (LQR) and LQR based on a Takagi-Sugeno fuzzy model.

3.2.2.1 Full State Feedback

First of all, the dynamics of the system (2.5) is approximated by a first order Taylor expansion at the point $x_o^T = (0 \quad 0 \quad 0 \quad 0)$. The Taylor series of d variables can be expressed as

$$f(x_1, \dots, x_d) = \sum_{n_1=0}^{\infty}\sum_{n_2=0}^{\infty}\dots\sum_{n_d=0}^{\infty}\frac{(x_1 - x_{01})^{n_1}\dots(x_d - x_{0d})^{n_d}}{n_1!\dots n_d!}\left(\frac{\partial^{n_1+\dots+n_d} f}{\partial x_1^{n_1}\dots\partial x_d^{n_d}}\right)(x_{01}, \dots, x_{0d}).$$

If only the first order is consider

$$f(x_1, \dots, x_d) \approx f(x_{01}, \dots, x_{0d}) + \sum_{j=1}^{d}\left(\frac{\partial f}{\partial x_j}\bigg|_{x=x_0}\right)(x_j - x_{0j}).$$

Rewriting the system (2.5) as $\dot{x} = f(x) + g(x)u$, we obtain a linear model such that

$$\dot{x} = Ax + Bu = \left.\begin{pmatrix} \frac{\partial f_1}{\partial x_1} & \frac{\partial f_1}{\partial x_2} & \frac{\partial f_1}{\partial x_3} & \frac{\partial f_1}{\partial x_4} \\ \frac{\partial f_2}{\partial x_1} & \frac{\partial f_2}{\partial x_2} & \frac{\partial f_2}{\partial x_3} & \frac{\partial f_2}{\partial x_4} \\ \frac{\partial f_3}{\partial x_1} & \frac{\partial f_3}{\partial x_2} & \frac{\partial f_3}{\partial x_3} & \frac{\partial f_3}{\partial x_4} \\ \frac{\partial f_4}{\partial x_1} & \frac{\partial f_4}{\partial x_2} & \frac{\partial f_4}{\partial x_3} & \frac{\partial f_4}{\partial x_4} \end{pmatrix}\right|_{x=x_0} \cdot x + \left.\begin{pmatrix} \frac{\partial g_1}{\partial x_1} \\ \frac{\partial g_2}{\partial x_1} \\ \frac{\partial g_3}{\partial x_1} \\ \frac{\partial g_4}{\partial x_1} \end{pmatrix}\right|_{x=x_0} \cdot u \qquad (3.1)$$

being

$$A = \begin{pmatrix} 0 & 0 & 1 & 0 \\ 0 & 0 & 0 & 1 \\ 0 & 73.0 & -42.8 & -0.90 \\ 0 & 118.1 & -40.8 & -1.46 \end{pmatrix}, B = \begin{pmatrix} 0 \\ 0 \\ 77.87 \\ 77.67 \end{pmatrix}. \qquad (3.2)$$

The feedback gain is designed to reach some desired poles. For this reason, the characteristic polynomial of A is computed:

$$s^n + a_n s^{n-1} + \cdots + a_1 = 0,$$

being in this case $n = 4$ the number of the states of the system. The transpose companion matrix [58] of A can be found as:

$$\tilde{A} = \begin{pmatrix} 0 & 1 & \dots & 0 & 0 \\ 0 & 0 & \dots & 0 & 0 \\ \vdots & \vdots & \ddots & \vdots & \vdots \\ 0 & 0 & \dots & 0 & 1 \\ -a_1 & -a_2 & \dots & -a_{n-1} & -a_n \end{pmatrix},$$

and the matrix

$$\tilde{B} = \begin{pmatrix} 0 \\ \vdots \\ 0 \\ 1 \end{pmatrix}.$$

Next, the characteristic polynomial of the system $\tilde{A} + \tilde{B}\tilde{K}$ is calculated:

$$\tilde{A} + \tilde{B}\tilde{K} = \begin{pmatrix} 0 & 1 & \dots & 0 & 0 \\ 0 & 0 & \dots & 0 & 0 \\ \vdots & \vdots & \ddots & \vdots & \vdots \\ 0 & 0 & \dots & 0 & 1 \\ -a_1 + \tilde{k}_1 & -a_2 + \tilde{k}_2 & \dots & -a_{n-1} + \tilde{k}_{n-1} & -a_n + \tilde{k}_n \end{pmatrix}.$$

According with Quanser specifications [59], the damping ratio and the natural frequency are $\zeta = 0.7$ and $\omega_n = 4\, rad/s$, respectively. Thus, the desired poles are selected as

$$p = (-40 \quad -30 \quad -2.80 \pm 2.86i),$$

which yields

$$\widetilde{K} = -(19200 \quad 9835 \quad 1707 \quad 29).$$

Finally it is obtained:

$$K_{FSF} = \widetilde{K}W^{-1} = -(-5.26 \quad 28.16 \quad -2.76 \quad 3.22),$$

where $W = T\tilde{T}^{-1}$ and

$$T = [B \quad AB \quad A^2B \quad \cdots \quad A^nB]$$
$$\tilde{T} = [\tilde{B} \quad \tilde{A}\tilde{B} \quad \tilde{A}^2\tilde{B} \quad \cdots \quad \tilde{A}^n\tilde{B}]$$

are the controllability matrices.

If this feedback gain is applied for the stabilization of the pendulum, we can use a simulation to compute the largest region of attraction. This region is defined by the maximum α which allows the correct switch between the swing-up and the stabilization control. In this case, $\alpha = 37.2°$. The results of the simulation are shown in the Figure 3.1.

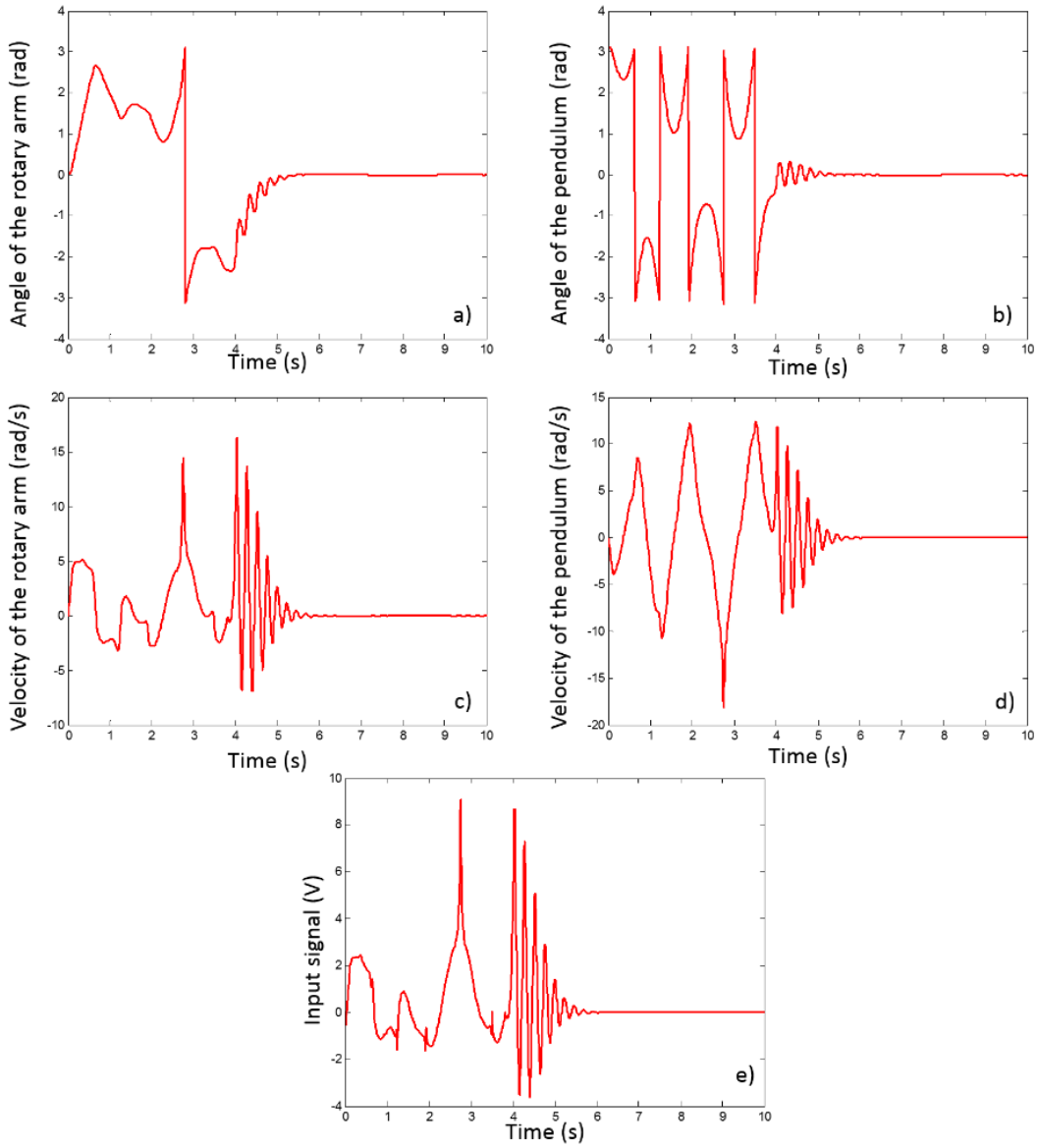

Figure 3.1: Simulation of the RIP using the FSF controller for the stabilization. a) Angle described by the rotary arm. b) Angle described by the pendulum. c) Velocity of the rotary arm. d) Velocity of the pendulum. e) Input signal

3.2.2.2 Linear Quadratic Regulator

The LQR approach is an optimal control technique which consists of minimizing the cost function given the system (3.1):

$$J = \int_0^\infty x(t)^T Q x(t) + u(t)^T R u(t) dt,$$

where Q and R are the weight matrices and indicate how LQR minimizes the function and the feedback gain is given by $K = R^{-1}B^T P$, where P is the unique positive defined solution of the algebraic Ricatti's equation:

$$A^T P + PA - PBR^{-1}B^T P + Q = 0.$$

The choice of the weight matrices is done using the Bryson's rules [60]:

$$Q_{ii} = \frac{1}{maximum\ acceptable\ value\ of\ x_i^2}$$

$$R_{jj} = \frac{1}{maximum\ acceptable\ value\ of\ u_j^2}.$$

Thus,

$$Q = \begin{pmatrix} 8.16 & 0 & 0 & 0 \\ 0 & 8.16 & 0 & 0 \\ 0 & 0 & 4 & 0 \\ 0 & 0 & 0 & 4 \end{pmatrix}$$

$$R = 1$$

This yields the following feedback gain:

$$K_{LQR} = -(-2.86 \quad 32.14 \quad -2.37 \quad 3.86).$$

In the same way that in the previous subsection, the maximum α for LQR is $40.1°$. The evolution of the states and the control signal are depicted in the Figure 3.2.

3.2.2.3 Control based on Takagi-Sugeno fuzzy model

The fuzzy model, which is proposed by *Takagi and Sugeno* [61], is described by means of a succession of IF-THEN rules that represent the local input-output relations of a nonlinear system, in such way that each rule expresses the local dynamic by a linear system [62]:

Rule i: if x_1 is equal to M_1^i, … and x_n is equal to M_n^i, then $\dot{x} = f_i(x)$.

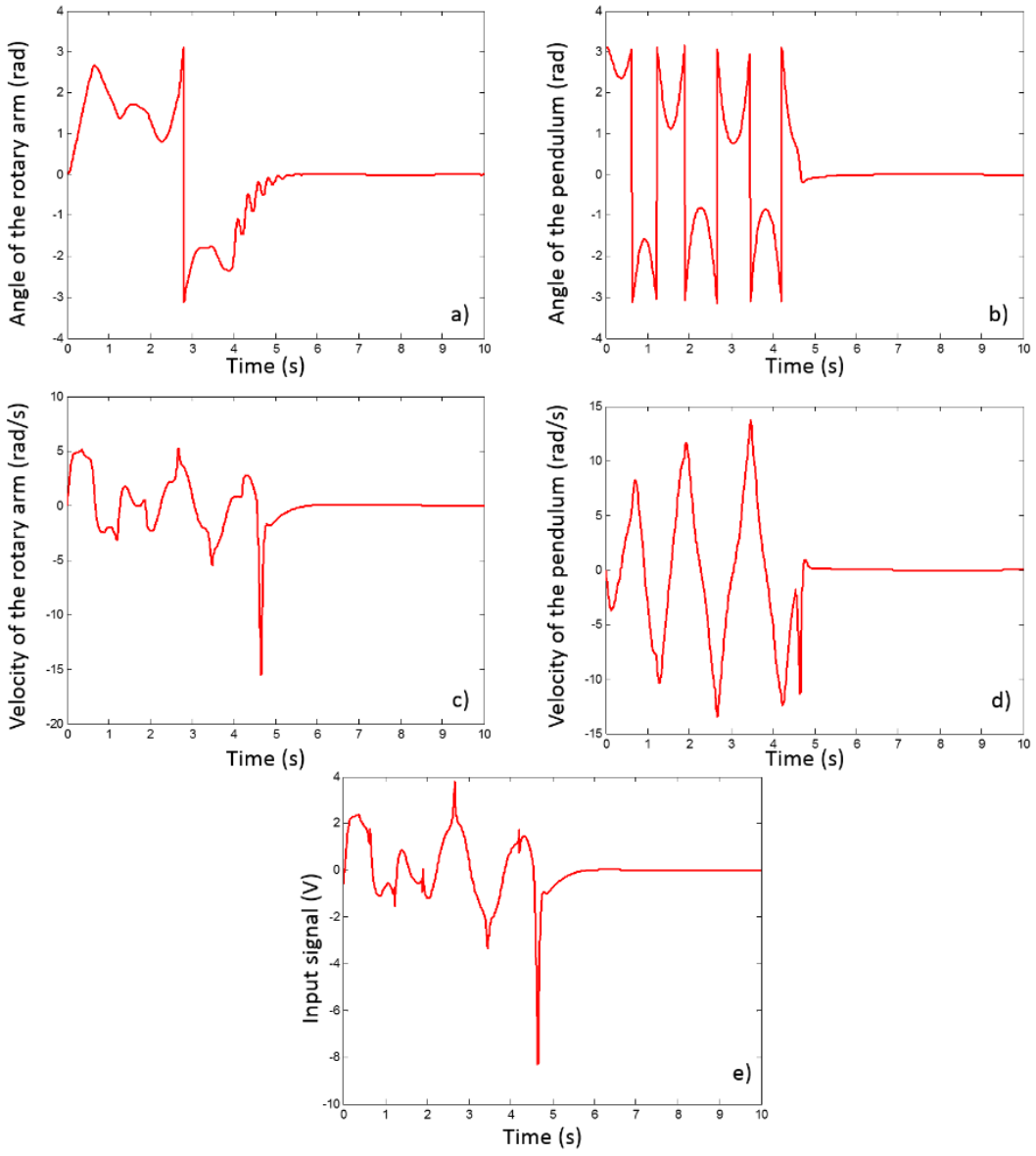

Figure 3.2: Simulation of the RIP using the LQR controller for the stabilization. a) Angle described by the rotary arm. b) Angle described by the pendulum. c) Velocity of the rotary arm. d) Velocity of the pendulum. e) Input signal

Therefore, the output of the fuzzy model for any x is the following:

$$\dot{x} = \frac{\sum_{j=1}^{m} w_j f_j(x)}{\sum_{j=1}^{m} w_j},$$

where

$$w_j = M_1^j \dots M_n^j,$$

being M_i^j the membership functions and $f_j(x)$ the consequence for each rule [61].

For the construction of the fuzzy model, the membership function M_i^j can be taken such that they are divided in M_i and $\bar{M}_i$ as it is shown in Figure 3.3.

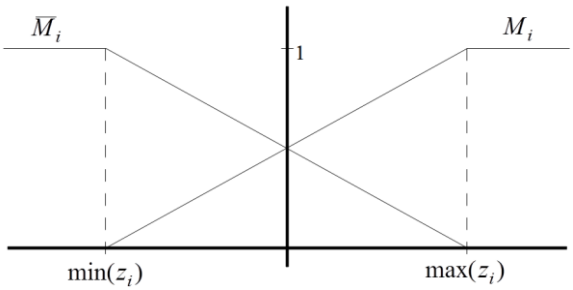

Figure 3.3: Membership functions construction

Note that the relation $M_i + \bar{M}_i = 1$ is preserved and that M_i is 0 if $z_i < \min(z_i)$ and 1 if $z_i > \max(z_i)$ (and the opposite for $\bar{M}_i$). Writing the variables z_i in terms of these membership functions as

$$z_i = M_i\, max(z_i) + \bar{M}_i\, min(z_i),$$

where $\max(z_i)$ and $\min(z_i)$ are the maximum and minimum value, respectively, that the variable z_i can reach. For instance, in the model presented in Section 2.2, the maximum and minimum values are presented in Table 3.1.

Table 3.1: Maximum and minimum values of the variables z_i.

Variables	Maximum value	Minimum value
z_1	1	0.9003
z_2	1	0.7071
z_3	6	-6
z_4	4.2426	-4.2426

So we can establish the 16 rules as follows:

Rule 1: If z_1 is equal to $\bar{M}_1$, z_2 is equal to $\bar{M}_2$, z_3 is equal to $\bar{M}_3$ y z_4 is equal to $\bar{M}_4$ then $\dot{x} = A_1 x + B_1 u$.

Rule 2: If z_1 is equal to $\bar{M}_1$, z_2 is equal to $\bar{M}_2$, z_3 is equal to $\bar{M}_3$ y z_4 is equal to M_4 then $\dot{x} = A_2 x + B_2 u$.

…

Rule 16: If z_1 is equal to M_1, z_2 is equal to M_2, z_3 is equal to M_3 y z_4 is equal to M_4 then $\dot{x} = A_{16}x + B_{16}u$.

Hence, the 16 rules provide 16 A matrices and 16 B matrices with constant elements. That is, a fuzzy technique is applied in order to obtain 16 linear systems and their 16 corresponding feedback gains. As a result, after the defuzzication process, the gain K applied to the nonlinear system can be computed from

$$u(t) = -\frac{\sum_{j=1}^{16} w_j K_j x(t)}{\sum_{j=1}^{16} w_j} = -K_{FZ}x(t), \qquad (3.3)$$

where $w_1 = \bar{M}_1\bar{M}_2\,\bar{M}_3\bar{M}_4$, $w_2 = \bar{M}_1\bar{M}_2\,\bar{M}_3M_4$, … , $w_{16} = M_1M_2M_3M_4$.

Thus, using the LQR design explained in Subsection 3.2.2.2, and using the same matrices Q and R, we compute 16 K_i gains for the 16 states defined by (A_i, B_i). Finally, using (3.3), the "overall system" gain applied is:

$$K_{FZ} = -(-2.86 \quad 22.22 \quad -2.28 \quad 3.99)$$

Simulating the system with the feedback gain for the fuzzy controller, we observe that the region of attraction has grown up. In this case, the switch between the swing-up and the stabilization is produced in $\alpha = 51.6°$. The evolution of the states and the input signal are presented in the Figure 3.4.

The results of the simulations are summarized in the Table 3.2.

Table 3.2: Comparison of the maximum region of attraction of the different stabilization control strategies for the RIP in simulation.

Strategy	Maximum region of attraction	Improvement of LQR based on TS
FSF	±37.2°	38.7%
LQR	±40.1°	28.7%
LQR based on TS	±51.6°	-

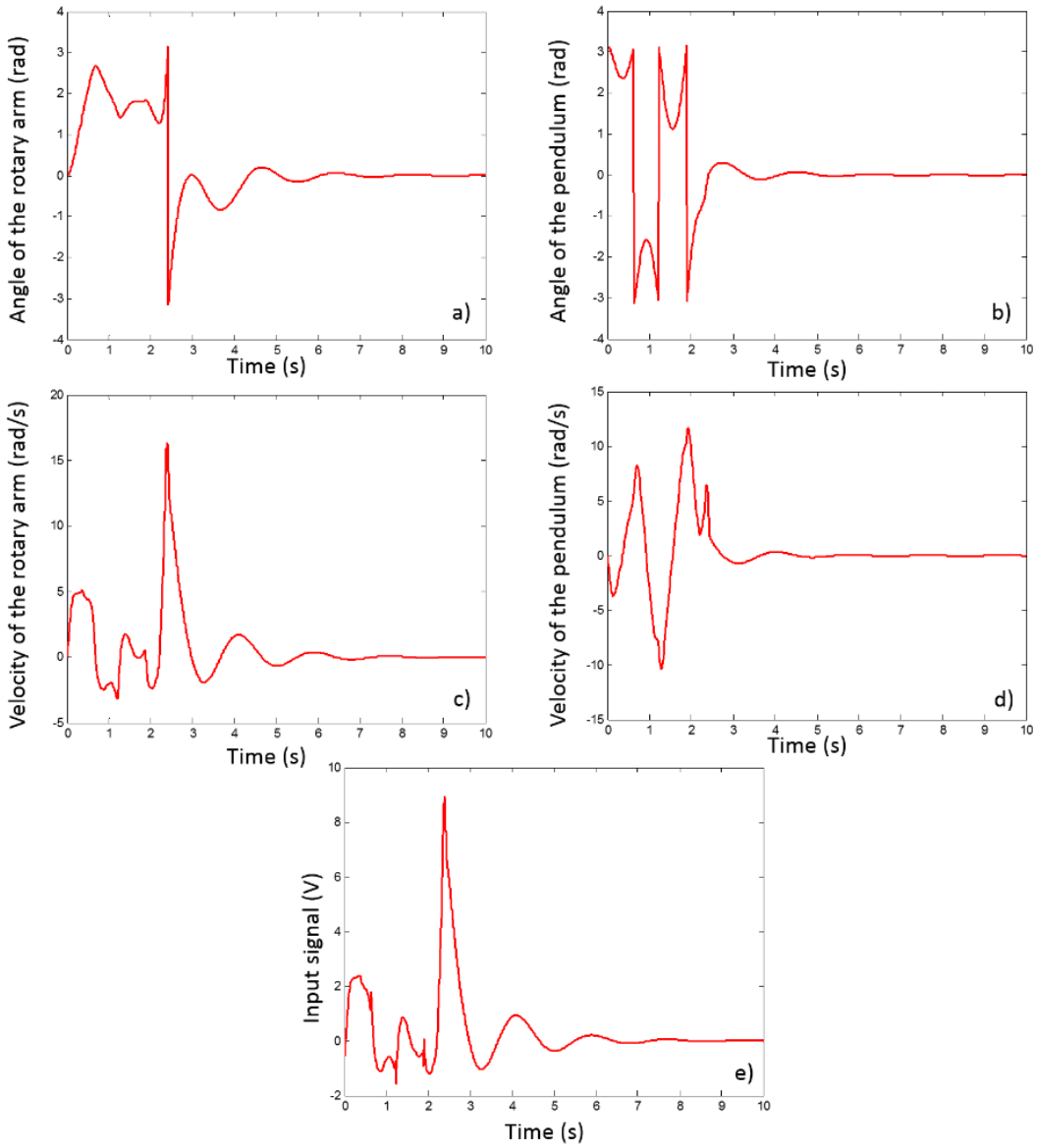

Figure 3.4: Simulation of the RIP using the fuzzy controller for the stabilization. a) Angle described by the rotary arm. b) Angle described by the pendulum. c) Velocity of the rotary arm. d) Velocity of the pendulum. e) Input signal

3.3 Double Rotary Inverted Pendulum

In the case of the DRIP, the swing up control is considerably more complex and the design of the plant is not devised for this kind of experiment. For this reason, the control strategy only includes the stabilization control. A LQR has been taken as in the subsection 3.2.2.2 for the RIP. First of all, it is necessary to linearize the system (2.6). The equations obtained are:

$$\begin{pmatrix} J_r L_r^2(m_s+m_h+m_p) & -L_r(m_s l_s+m_h L_s+m_p L_s) & m_p l_p L_r \\ -L_r(m_s l_s+m_h L_s+m_p L_s) & J_s+m_s l_s^2+m_h L_s^2+m_p L_p^2 & m_p l_p L_s \\ -m_p l_p L_r & m_p l_p L_s & J_p+m_p l_p^2 \end{pmatrix}\begin{pmatrix}\ddot{\theta}\\ \ddot{\alpha}\\ \ddot{\gamma}\end{pmatrix}$$
$$= \begin{pmatrix} 0 & 0 & 0 & -B_r & 0 & 0 \\ 0 & -g(m_s l_s+m_h L_s+m_p L_s) & 0 & 0 & -B_s & 0 \\ 0 & 0 & g m_p l_p & 0 & 0 & -B_p \end{pmatrix}\begin{pmatrix}\theta\\ \alpha\\ \gamma\\ \dot{\theta}\\ \dot{\alpha}\\ \dot{\gamma}\end{pmatrix} + \begin{pmatrix}\tau\\ 0\\ 0\end{pmatrix} \quad (3.4)$$

Multiplying by

$$H = \begin{pmatrix} J_r L_r^2(m_s+m_h+m_p) & -L_r(m_s l_s+m_h L_s+m_p L_s) & m_p l_p L_r \\ -L_r(m_s l_s+m_h L_s+m_p L_s) & J_s+m_s l_s^2+m_h L_s^2+m_p L_p^2 & m_p l_p L_s \\ -m_p l_p L_r & m_p l_p L_s & J_p+m_p l_p^2 \end{pmatrix}^{-1}$$

in both sides of (3.4), a linear model is obtained:

$$\begin{pmatrix}\ddot{\theta}\\ \ddot{\alpha}\\ \ddot{\gamma}\end{pmatrix} = H\begin{pmatrix} 0 & 0 & 0 & -B_r & 0 & 0 \\ 0 & -g(m_s l_s+m_h L_s+m_p L_s) & 0 & 0 & -B_s & 0 \\ 0 & 0 & g m_p l_p & 0 & 0 & -B_p \end{pmatrix}\begin{pmatrix}\theta\\ \alpha\\ \gamma\\ \dot{\theta}\\ \dot{\alpha}\\ \dot{\gamma}\end{pmatrix} + H\begin{pmatrix}\tau\\ 0\\ 0\end{pmatrix}.$$

Replacing the parameters, the (A, B) matrices of the state-space representation result:

$$A = \begin{pmatrix} 0 & 0 & 0 & 1 & 0 & 0 \\ 0 & 0 & 0 & 0 & 1 & 0 \\ 0 & 0 & 0 & 0 & 0 & 1 \\ 0 & 290.97 & -15.85 & -46.67 & -0.75 & 1 \\ 0 & 256.47 & -28.90 & -35.57 & -0.70 & 1.15 \\ 0 & -339.91 & 127.44 & 47.14 & 1.15 & -3.11 \end{pmatrix}, B = \begin{pmatrix} 0 \\ 0 \\ 0 \\ 84.95 \\ 64.77 \\ -85.84 \end{pmatrix}.$$

Finally, using LQR as in subsection 3.2.2.2, with the following weight matrices

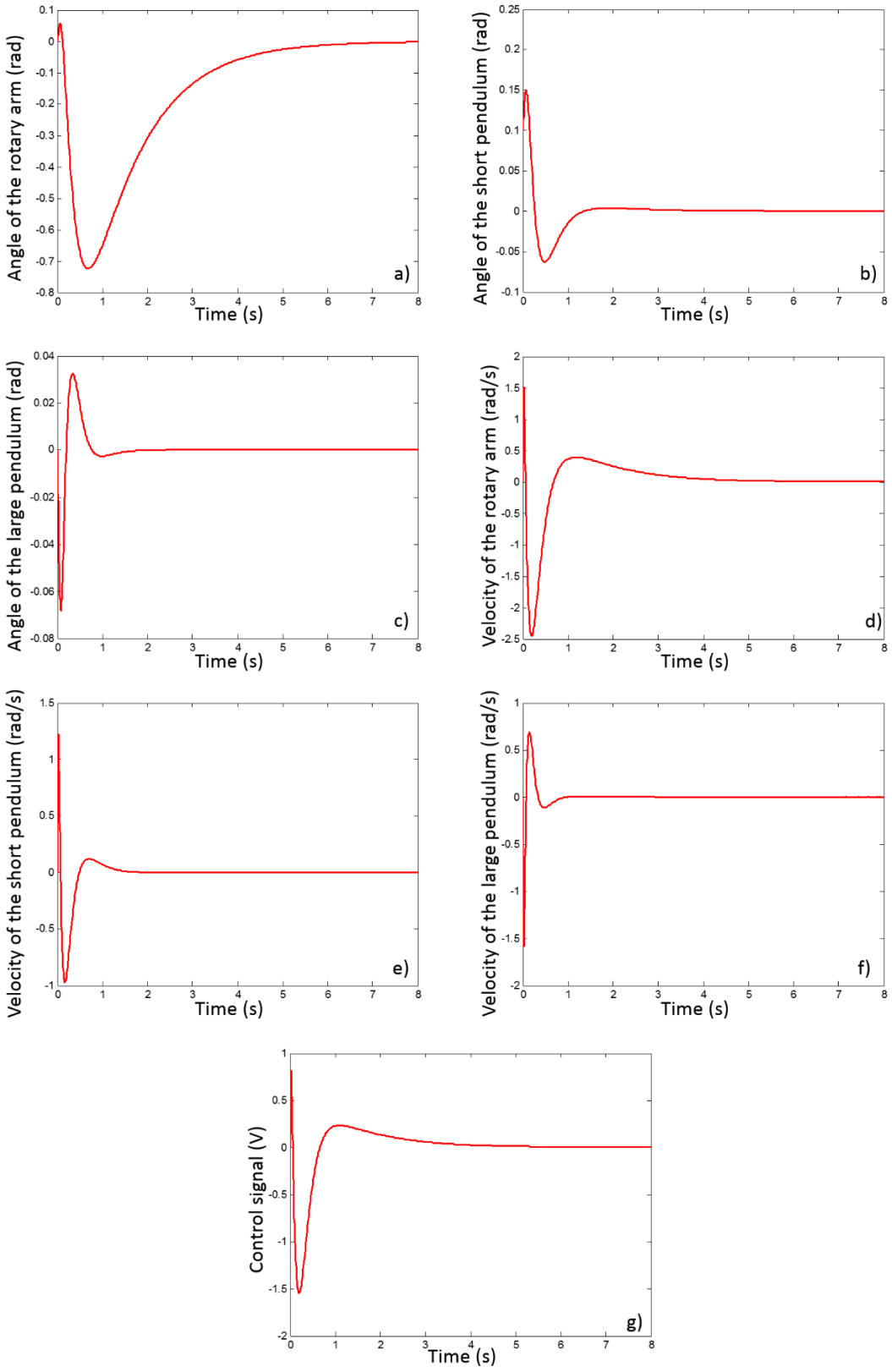

Figure 3.5: Simulation of the stabilization control of the DRIP. a)-c) Angles described by the rotary arm and the pendulums. d)-f) Velocities of the rotary arm and the pendulums. g) Control signal

$$Q = \begin{pmatrix} 1 & 0 & 0 & 0 & 0 & 0 \\ 0 & 1 & 0 & 0 & 0 & 0 \\ 0 & 0 & 1 & 0 & 0 & 0 \\ 0 & 0 & 0 & 5 & 0 & 0 \\ 0 & 0 & 0 & 0 & 1 & 0 \\ 0 & 0 & 0 & 0 & 0 & 1 \end{pmatrix}, R = 30,$$

the following feedback gain results:

$$K_D = -(0.54 \quad -20.48 \quad -55.90 \quad 0.45 \quad -7.32 \quad -5.63).$$

The correct work of the feedback gain has been tested in simulation. We can see in the Figure 3.5 that the DRIP reaches the equilibrium when the initial conditions are close to the linearization point. In this case, $x_0^T = (0 \quad 0.1 \quad 0 \quad 0 \quad 0 \quad 0)$.

4. SAMPLING AND CONTROL TASK UPDATE

4.1 Introduction

In this section, the different sampling strategies and ways to update the control signal are proposed. First, the Time Driven Control (TDC) is introduced. The stability of uniformly sampled systems has been widely studied [63], [64], [65]. Nevertheless, the ETC and PETC are proposed to get a best use of resources. The three strategies are illustrated through an example (a DC motor) and the corresponding results are compared. Finally, the theory is applied to the rotary inverted pendulum.

4.2 Time-Driven Control

The time-driven control samples the states and updates the control task periodically. The theory of sampled-data system has been well-developed [66], [67], [68] and it results very useful for the analysis and design of the system. However, it is less preferable from a resource utilization point of view [10].

In sampled data control, the control law can be represented as a delayed input as follows:

$$u(t) = u_d(t_k) \; with \; t_k \leq t < t_{k+1}, \quad k \in \mathbb{N}$$

where $u_d(t_k)$ is the discrete-time control signal and the delay is piecewise continuous and defined as $\delta(t) = t - t_k, k \in \mathbb{N}$. In this way, the linearized system (3.1) can be rewritten as

$$\dot{x} = Ax + BKx(t_k). \tag{4.1}$$

The sampling period h is such that $h = t_{k+1} - t_k \; \forall k \geq 0$ and it is constant. It can be computed employing the Nyquist-Shannon sampling theorem [69].

Example 4.1: Consider a linear system of the form:

$$\begin{cases} \dot{x} = Ax + Bu \\ y = Cx + Du \end{cases} \tag{4.2}$$

with

$$A = \begin{pmatrix} -0.5 & 0 \\ 1 & 0 \end{pmatrix}$$
$$B = \begin{pmatrix} 1 \\ 0 \end{pmatrix}$$
$$C = (-0.54 \quad 0) \qquad (4.3)$$
$$D = 0$$

which correspond to the (stable) second-order linear model of a motor. The sampling period using the Nyquist-Shannon sampling theorem is $h = 0.1\ s$. We can compute the discrete model of the system for this sampling period such that

$$A_d = \begin{pmatrix} 0.95 & 0 \\ 0.097 & 1 \end{pmatrix}$$
$$B_d = \begin{pmatrix} 0.097 \\ 0.0049 \end{pmatrix}$$
$$C_d = (-0.54 \quad 0)$$
$$D_d = 0$$

Thus,

$$x_{k+1} = A_d x_k + B_d u(t_k),$$

where $x_k = x(t_k)$ and $x_{k+1} = x(t_{k+1})$. We compute a feedback gain using a LQR design so that the closed-loop system is stable. For a sampling period $h = 0.1\ s$, the number of samplings per second is 10. The state of the system and the number of control updates is depicted in Figure 4.1.

4.3 Event-Triggered Control

The idea of a control based on events came up to reduce the waste of communication resources, because it has been proved to reduce the number of transmission from the sensor to the controller (and/or from the controller to the actuator) in the classical time-driven control. Event based systems are characterized by

an event-triggering condition, which determines when the input signal is updated. The EBC can be implemented in many ways [7], but the common idea is to define an error function and a threshold to bound the error.

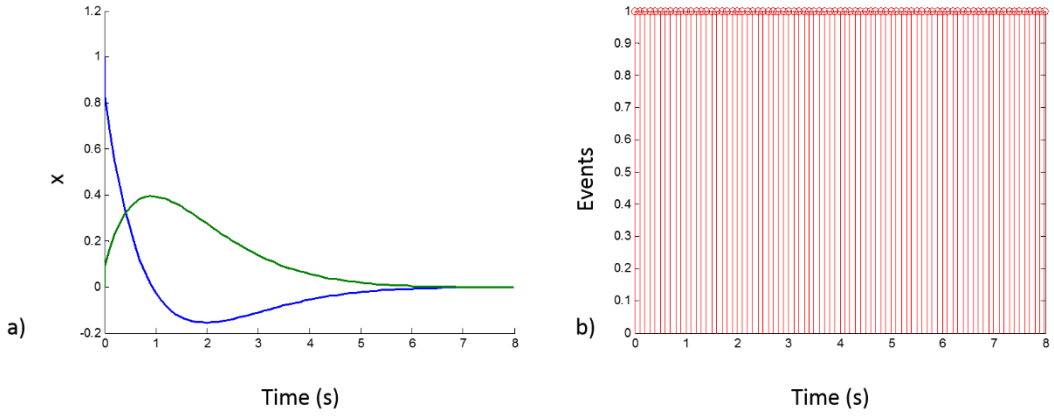

Figure 4.1: Simulation of the motor with TDC. In (a) the evolution of the state is represented. In blue x_1 and in green x_2. In (b) each vertical line correspond to an event. Since the control task is periodically updated, there is an event each 0.1s

If the error is the difference between the state at the last event occurrence and the current state and the bound is constant, it is called deadband control [39], [70] and the triggering condition is (see Figure 4.2 a,b):

$$\|e(t)\| \leq c$$

However, the deadband control does not generally guarantee asymptotic stability. For this reason, others conditions have been studied. For example, bounding the error with the state [9]:

$$\|e(t)\| \leq \sigma \|x(t)\|$$

Recently, trigger rules depending on the time have been proposed in order to reach the reference asymptotically [71], [72]:

$$\|e(t)\| \leq c_1 e^{-\alpha_1 t}$$

It can be defined also from the Lyapunov function [40] (see Figure 4.2 c):

$$V(x,t) \leq S(x,t)$$

where $S(x,t)$ is a certain threshold of reference.

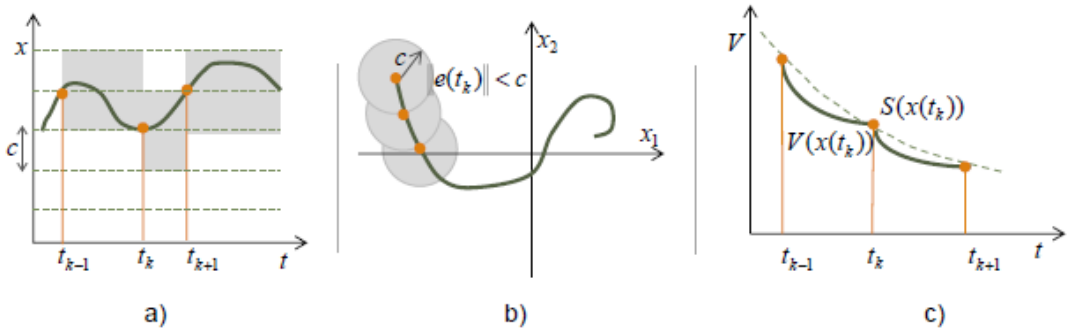

Figure 4.2: Different trigger rules. Figure from [7]

In this master thesis, an event-triggering condition proportional to the norm of the state is studied:

$$\|e(t)\| \leq \sigma \|x(t)\|, \tag{4.4}$$

where σ is a parameter such that $0 < \sigma < 1$, and $e(t)$ is the error between the state in the last control update and the current state. So, it is defined as:

$$e(t) = x(t_k) - x(t),$$

and it is compared with a constant event-triggering condition:

$$\|e(t)\| \leq c, \tag{4.5}$$

where c is a constant maximum value to determine.

Consider now the following linear system and the first event condition proposed:

$$\dot{x}(t) = Ax + BK(e(t) + x(t)) \tag{4.6}$$

With a similar procedure to [73], where a method to obtain the maximum σ for event-triggered output-feedback is presented, it is possible to guarantee the stability of the system. First of all, let us define a proposition whose result will be used in the future.

Proposition 4.1: Consider $n \times n$ matrices a and b and consider $\psi > 0$, also a $n \times n$ matrix. Then:

$$2a^T b \leq a^T \psi a + b^T \psi^{-1} b.$$

Proof: This can be shown choosing a matrix $M^* > 0$, such that $M^* = M^T M$, by definition of positive definite matrix. Then, if $M = (\phi a \phi^{-1} + \phi^{-1} b \phi)$, and ϕ is positive definite:

$$(\phi a \phi^{-1} + \phi^{-1} b \phi)^T (\phi a \phi^{-1} + \phi^{-1} b \phi) > 0.$$

Computing the product, using that

$$a^T \phi \phi a + b^T \phi^{-1} \phi^{-1} b - 2a^T b > 0$$

for a positive definite matrix $= \phi^T$, replacing $\phi\phi = \psi$ and extending the result to the case in which $a = b$, the proof is completed. ■

Now we can formulate the theorem which guarantees the asymptotic stability of a linear system under the event condition (4.4).

Theorem 4.1: The system (4.6) is asymptotically stable under the condition (4.4) if there exist a positive definite matrix P and a positive scalar σ such that the inequality (4.7) is satisfied:

$$PA_k + A_k^T P + PBK(PBK)^T + \sigma^2 < 0, \qquad (4.7)$$

being $A_k = A + BK$.

Proof: Choose $V = x^T(t)Px(t)$ as a Lyapunov function candidate. If $P > 0$, then V is a positive definite function. Then compute its derivate:

$$\dot{V} = \dot{x}^T(t)Px(t) + x^T(t)P\dot{x}(t) = x^T(t)(PA_k + A_k^T P)x(t) + 2x^T(t)PBKe(t).$$

Keeping in mind the Proposition 4.1 and taking $a^T = x^T(t)PBK$, $b = e(t)$ and $\psi = I$. Then

$$\dot{V} \leq x^T(t)(PA_k + A_k^T P + PBK(PBK)^T)x(t) + e^T(t)e(t).$$

Since $e^T(t)e(t) \leq \sigma^2 x^T(t)x(t)$ holds, replacing $e^T(t)e(t)$ by $\sigma^2 x^T(t)x(t)$:

$$\dot{V} \leq x^T(t)(PA_k + A_k^T P + PBK(PBK)^T + \sigma^2)x(t),$$

and considering that $\dot{V} < 0$ must hold for asymptotic stability (Lyapunov's second method [57]):

$$PA_k + A_k^T P + PBK(PBK)^T + \sigma^2 < 0$$

and this completes the proof. ■

Remark: Note that the inequality (4.7) is nonlinear due to the third term. However, it can be transformed in a Linear Matrix Inequality (LMI) using the Schur complement [74]:

$$\begin{pmatrix} PA_k + A_k^T P + \sigma^2 & PBK \\ (PBK)^T & -I \end{pmatrix} < 0.$$

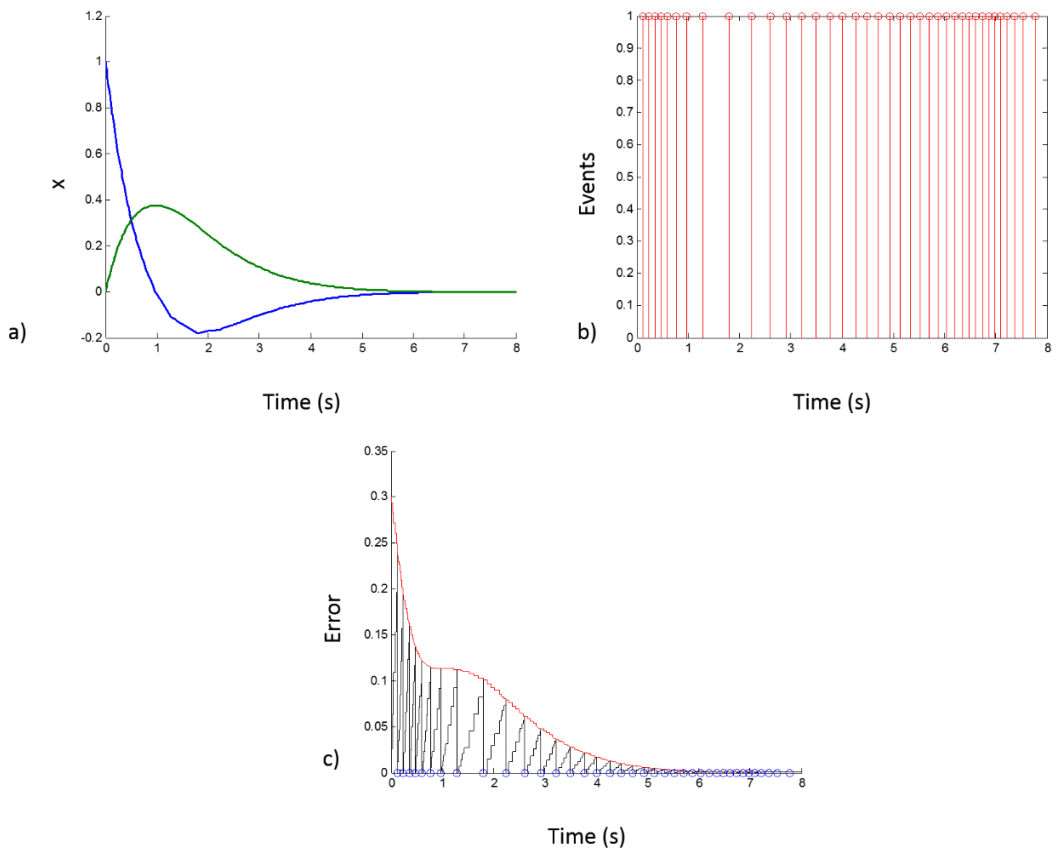

Figure 4.3: Simulation of the motor with ETC with condition (4.4). (a) The evolution of the state variables. In blue x_1 and in green x_2. In (b) each vertical line correspond to an event. The more the state is close to zero, more events happen. (c) In black the evolution of the norm of the error. In red, the bound determined by the event condition (4.4)

Example 4.2: Consider again the continuous system (4.2), (4.3) and the event condition (4.4). If we compute again a feedback gain K using, for example, a LQR and

we apply the Theorem 4.1, the result is that the system can be asymptotic stabilized to the origin if the parameter σ satisfies $\sigma < 0.6$. We can take for instance $\sigma = 0.3$ in order to check the result.

In the Figure 4.3a, we can see that the behaviour of the state is very similar to the presented one in the case of time-driven control. However, in this case, the signal input has been only updated 38 times. That is a reduction of 52.5%. Figure 4.3b illustrates how the events are more and more frequent when the state is closer to zero.

Moreover, we can see in the Figure 4.3c how the error increases with time until it reaches the bound. Then the control task is updated and the error goes back to zero.

We can compare this result with the constant event-triggering condition (4.5), choosing for example $c = 0.03$. The Figure 4.4 shows that the system is not asymptotically stable even when it is simulated for a long time ($100s$). Besides, 54 events have been produced in $8\ s$, a higher number than in the case of the condition (4.4). Respect to the time-driven control, the number of samplings is reduced in 32.5%.

4.4 Periodic Event-Triggered Control

The idea of the PETC, as already mentioned, is join the advantages of time-sampled control and event-triggered control to reduce the waste of communication and computation resources. The Periodic Event-Triggered Control has been studied by *Heemels et al.* [10] for linear systems and more recently for nonlinear systems [36].

In this master thesis, one of the principal aims is to obtain a novel way to determine the maximum period that guarantees the stability of the system and the boundedness of the error due to the even-triggering. Note that, in general, when choosing a period and an event-triggering condition the system can be stable but the second condition usually does not hold. That is, the event occurs between the times t_k and t_{k+1} but it is not detected until t_{k+1} (see Figure 4.5).

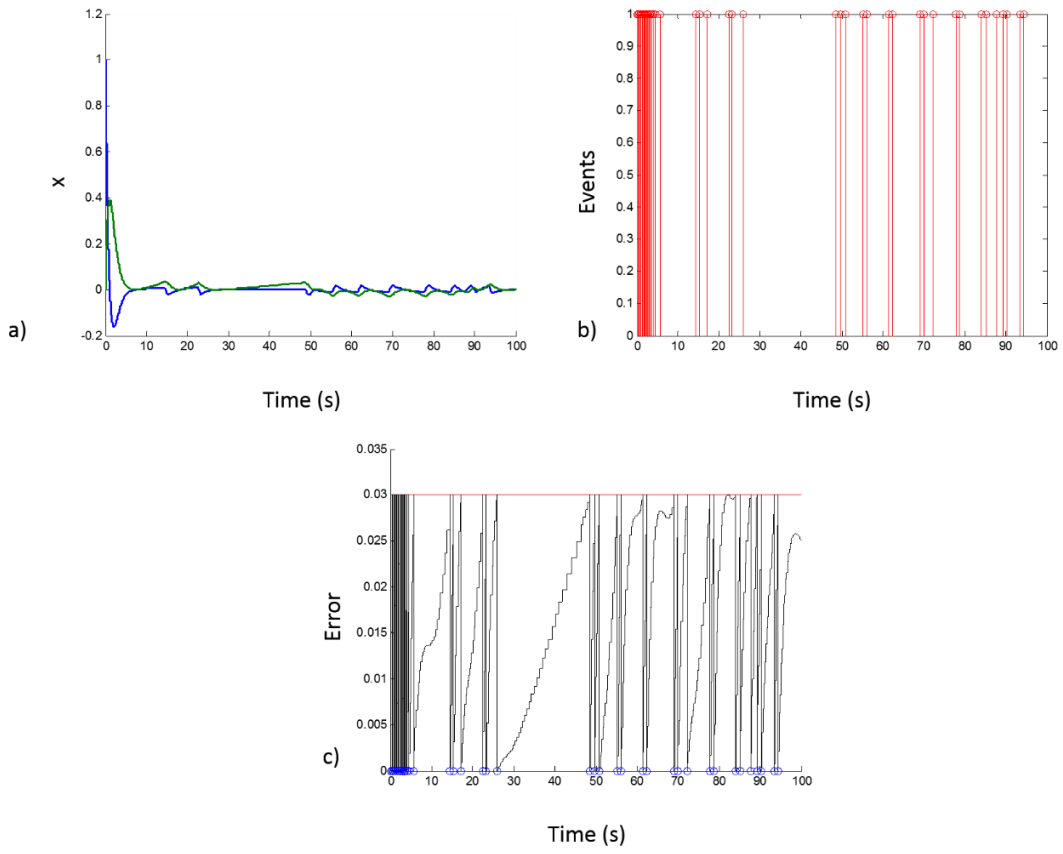

Figure 4.4: Simulation of the motor with ETC with condition (4.5). (a) The evolution of the state variables. In blue x_1 and in green x_2. In (b) each vertical line correspond to an event. (c) In black the evolution of the norm of the error. In red, the constant bound in 0.03 determined by the event condition (4.5)

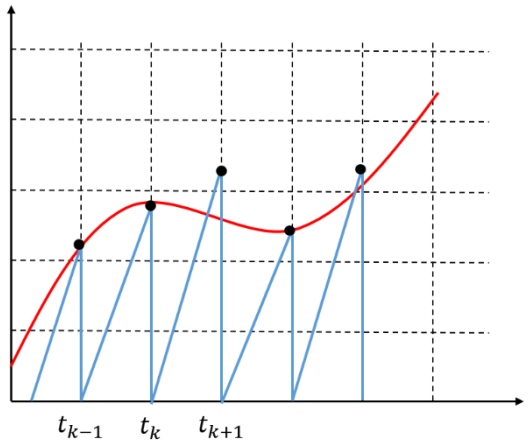

Figure 4.5: Scheme of the situation when the time between an event and another is less than the sampling period. The error is represented in blue and the threshold in red

With this aim in mind, the theory established for the ETC is extended to the PETC.

Let us formulate the following proposition, which is derived from the Razumikhin theorem [75], the improvement made by B. Xu and Y. Liu [76], and the corrections of X. Mao [77], and that will be used in the future.

Proposition 4.2: A time-delay system with maximum time-delay h is asymptotically stable if there exists a bounded quadratic Lyapunov function V such that for some $\varepsilon > 0$, it satisfies

$$V(x) \geq \varepsilon \|x\|^2$$

and its derivative along the system trajectory, $\dot{V}(x(t))$, satisfies

$$\dot{V}\big(x(t)\big) \leq -\varepsilon \|x\|^2$$

and there is a $q_2 \geq 1/q_1$ such that

$$\sup_{\xi \in [-h,0]} V\big(t+\xi, x(t+\xi)\big) < q_1 V\big(t, x(t)\big)$$

at any $t \geq t_0$ implies

$$\sup_{\xi \in [-h,0]} \|x(t+\xi)\| \leq q_1 q_2 \|x(t)\| < u^{-1}\{q_1 v \|x(t)\|\}$$

at the same t whenever

$$\|x(t+\xi)\| \leq q\|x(t)\|, -h \leq \xi \leq 0$$

for some constant $q = q_1 q_2 > 1$.

This proposition is derived from the Razumikhin theorem, which can be found in the Appendix B.

Consider the linear system (4.6) and replace $e(t) + x(t)$ by $e(t_k) + x(t_k)$, because the event condition is only checked periodically at $t_k, k \in \mathbb{N}$. Finally, calling $\delta(t) = t - t_k$:

$$\dot{x}(t) = Ax(t) + BK(e\big(t - \delta(t)\big) + x(t - \delta(t))) \qquad (4.8)$$

Consider also the condition (4.4). Then, it is possible to formulate the theorem.

Theorem 4.2: Given the system (4.8), it is asymptotically stable under the condition (4.4), if there exist a positive definite matrix P, a positive scalar σ, scalars $q_1, q > 1$, and a positive period h such that the inequality (4.9) is satisfied:

$$-Q^* + hR^* < 0, \tag{4.9}$$

where the matrices Q^* and R^* are

$$Q^* = -[A_k^T P + PA_k + PBK(PBK)^T + \sigma^2 q] > 0$$
$$R^* = 2q_1 P + PBKAP^{-1}(PBKA)^T + P(BK)^2(P(BK)^2)^T + P(BK)^2 P^{-1}(P(BK)^2)^T + \sigma^2 q > 0.$$

Proof: Note now that $x(t-\tau(t))$ can be expressed as:

$$\begin{aligned} x\big(t-\tau(t)\big) &= x(t) - \int_{t-\tau(t)}^{t} \dot{x}(s)ds \\ &= x(t) - \int_{t-\tau(t)}^{t} Ax(s)ds - \int_{t-\tau(t)}^{t} BKx\big(t-\tau(t)\big)ds \\ &\quad - \int_{t-\tau(t)}^{t} BKe(t-\tau(t))\,ds \end{aligned}$$

Then (4.8) results:

$$\begin{aligned} \dot{x}(t) = Ax(t) + BKx(t) - BKA\int_{t-\tau(t)}^{t} x(s)ds - (BK)^2 x\big(t-\tau(t)\big)\tau(t) \\ - (BK)^2 e\big(t-\tau(t)\big)\tau(t) + BKe(t-\tau(t)) \end{aligned}$$

Choose now a candidate Lyapunov function as in the ETC case. That is, $V = x^T(t)Px(t)$, P positive definite, which is a bounded quadratic function and satisfies the first condition of the Proposition 4.2. Computing its derivative:

$$\begin{aligned} \dot{V} = x^T(t)(PA_k + A_k^T P)x(t) - \int_{t-\tau(t)}^{t} 2x^T(t)PBKAx(s)ds \\ - 2\tau(t)x^T(t)(P(BK)^2)x\big(t-\tau(t)\big) \\ - \tau(t)x^T(t)P(BK)^2 e\big(t-\tau(t)\big) + x^T(t)PBKe(t-\tau(t)) \end{aligned}$$

Using again the expression $2a^T b \leq a^T \psi a + b^T \psi^{-1} b$ (see Proposition 4.1) and noting that $\tau(t) \leq h$, each term is bounded and the period comes up explicitly.

- With $a^T = -x^T(t)PBKA$, $b = x(s)$, $\psi = P^{-1}$:

$$-\int_{t-\tau(t)}^{t} 2x^T(t)PBKAx(s)ds \leq \int_{t-\tau(t)}^{t} V(s)ds + h[x^T(t)PBKAP^{-1}(PBKA)^T]$$

- With $a^T = -x^T(t)P(BK)^2$, $b = x\big(t-\tau(t)\big)$, $\psi = P^{-1}$:

$$-2\tau(t)x^T(t)(P(BK)^2)x\big(t-\tau(t)\big) \leq h[x^T(t)P(BK)^2P^{-1}(P(BK)^2)^T + V(t-\tau(t))]$$

- With $a^T = -x^T(t)P(BK)^2$, $b = e\big(t-\tau(t)\big)$, $\psi = I$

$$-\tau(t)x^T(t)P(BK)^2e\big(t-\tau(t)\big) \leq h[x^T(t)P(BK)^2(P(BK)^2)^T + e^T(t-\tau(t))e(t-\tau(t))]$$

- With $a^T = -x^T(t)PBK$, $b = e\big(t-\tau(t)\big)$, $\psi = I$

$$x^T(t)PBKe(t-\tau(t)) \leq x^T(t)PBK(PBK)^Tx(t) + e^T(t-\tau(t))e(t-\tau(t))$$

Summarizing:

$$\begin{aligned}\dot{V} \leq x^T(t)(PA_k + A_k^TP)x(t) + \int_{t-\tau(t)}^{t} V(s)ds + x^T(t)PBK(PBK)^Tx(t) \\ + e^T\big(t-\tau(t)\big)e\big(t-\tau(t)\big) \\ + +h\big[x^T(t)PBKAP^{-1}(PBKA)^T \\ + x^T(t)P(BK)^2P^{-1}(P(BK)^2)^T + V\big(t-\tau(t)\big) \\ + x^T(t)P(BK)^2(P(BK)^2)^T + e^T(t-\tau(t))e(t-\tau(t))\big]\end{aligned}$$

Using the Proposition 4.2, the Lyapunov function can be bounded as $V(t+\xi) \leq q_1V(t)$ with some constant $q_1 > 1$. So the following terms can be bounded:

$$\int_{t-\tau(t)}^{t} V(s)ds \leq \int_{t-\tau(t)}^{t} qV\big(x(t)\big)ds \leq q_1hV(x(t))$$

$$V(x(t-\tau(t))) \leq q_1V(x(t))$$

In addition, the triggering condition (4.4) is introduced, so $e^T\big(t-\tau(t)\big)e\big(t-\tau(t)\big) \leq \sigma^2 x^T\big(t-\tau(t)\big)x\big(t-\tau(t)\big) \leq \sigma^2 q\|x(t)\|$. Finally, $\dot{V}$ is bounded:

$$\begin{aligned}\dot{V} \leq x^T(t)\{&PA_k + A_k^T P + PBK(PBK)^T + \sigma^2 q \\ &+ h[2q_1 P + PBKAP^{-1}(PBKA)^T + P(BK)^2 P^{-1}(P(BK)^2)^T \\ &+ P(BK)^2(P(BK)^2)^T + \sigma^2 q]\}x(t) = x^T(t)[-Q^* + hR^*]x(t) \\ &< 0\end{aligned}$$

The system is asymptotically stable if $\dot{V} < 0$. Then if (4.9) holds, the stability condition is fulfilled guaranteeing that no events happen if $t - t_k < h$. ■

Remark: Note that if $h \to 0$, then the Theorem 4.2 turns into the Theorem 4.1.

Remark: As in the Subsection 4.3, the condition (4.9) is nonlinear. To construct a LMI, let us multiply (4.9) by $S = P^{-1}$ on the right and the left:

$$\begin{aligned}&[SA_k^T + A_k S + BK(BK)^T + S\sigma^2 qS] \\ &\quad + h[2q_1 S + BKAS(BKA)^T + (BK)^2((BK)^2)^T \\ &\quad + (BK)^2 S((BK)^2)^T + S\sigma^2 qS] < 0\end{aligned} \qquad (4.10)$$

Then, employing the Schur complement:

$$\begin{pmatrix} SA_k^T + A_k S + BK(BK)^T + 2hq_1 S & S \\ +h[BKAS(BKA)^T + (BK)^2((BK)^2)^T + (BK)^2 S((BK)^2)^T] & \\ S & \dfrac{-I}{\sigma^2 q(1+h)} \end{pmatrix} < 0$$

Example 4.3: Consider once again the system (4.2)-(4.3) and let us take the parameter $\sigma = 0.3$ from the Example 4.2. Then, from the Theorem 4.2 the maximum period h which guarantees the asymptotic stability of the system and that (4.4) holds is $h = 0.16$. Taking, for instance, $h = 0.1$, the results of the Figure 4.6 are obtained.

4.5 Application to the Stabilization of the RIP

First, the time-driven control is applied. Using the Nyquist-Shannon theorem, we can determine a sampling period of $10\ ms$. Simulating the system (3.1)-(3.2) with any of the computed feedback gains, for example, K_{FSF}. The result is shown in Figure 4.7.

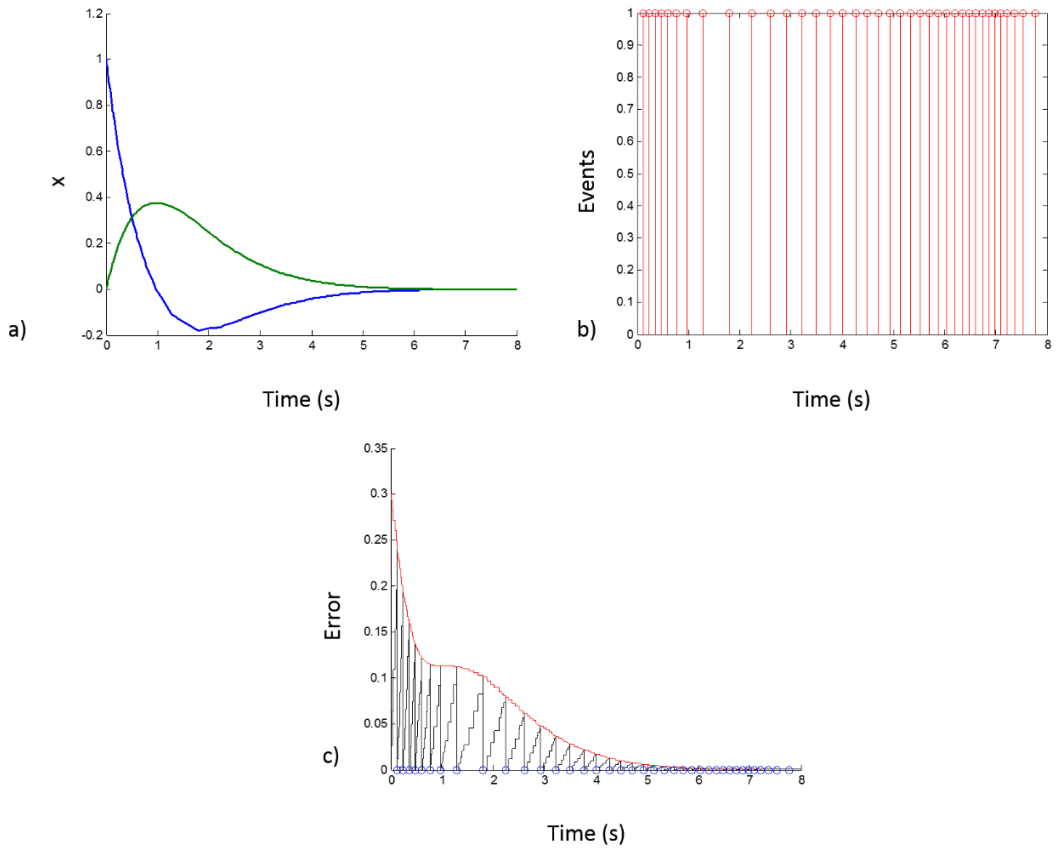

Figure 4.6: Simulation of the motor with PETC. (a) The evolution of the state variables. In blue x_1 and in green x_2. In (b) each vertical line correspond to an event. The closer the state is to zero, the shorter is the distance between events. (c) In black the evolution of the norm of the error. In red, the bound determined by the event condition (4.4)

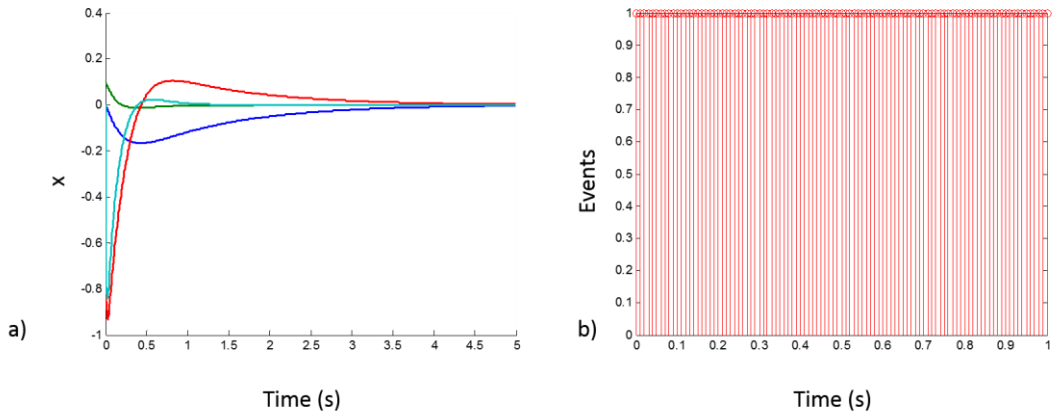

Figure 4.7: Simulation of the linear model of the RIP with gain K_{FSF}. In (a), the angle of the rotary arm is in blue, the angle of the pendulum in green, the angular velocity of the rotary arm in red and the angular velocity of the pendulum in cyan. (b) is a zoom between 0-1 seconds in order to observe that the events occur periodically

Consider the ETC, applying the results of the Theorem 4.1 for the system (4.6), being A and B the matricies of (3.2) and the feedback gains corresponding to the three stabilization methods, the following maximum σ are got (Table 4.1).

Table 4.1: Comparison between the maximum σ obtained for the different stabilization strategies. It is presented the maximum σ so that (4.7) holds. The last value of σ is the value for which (4.7) does not hold but if the inequality was ≥, then it would be feasible.

Strategy	Maximum σ feasible	Maximum σ not strictly feasible but may be feasible
FSF	0.0225	0.0377
LQR	0.0630	0.0699
LQR based on TS	0.0548	0.0599

If we simulate the system for the three gains with, for instance, $\sigma = 0.02$, $\sigma = 0.06$ and $\sigma = 0.05$, respectively, the number of events is clearly reduced in comparison with the TDC in the case of LQR and TS. However, the FSF controller in ETC present worse results than TDC because its maximum σ is more conservative (see Table 4.2). In the Figure 4.8 the evolution of the states and the error and the events are represented for the fuzzy control as an example. It can seem weird that more events happen when the system is far from the equilibrium. However, the reason for this is that the velocity of the pendulum increases very fast at the beginning because of the gravitational acceleration. When the pendulum is closer to the equilibrium, this effect is reduced.

Table 4.2: Comparison of the different strategies for the RIP using the ETC respect to the TDC in simulation.

Strategy	σ	Number of events	Reduction respect to the TDC
FSF	0.02	733	-83.25%
LQR	0.06	255	36.75%
LQR based on TS	0.05	289	27.75%

Next, these values of σ can be taken to determine the maximum period in the case of PETC. Solving the inequality of Theorem 4.2 for the system (4.8), the maximum h that results for the three stabilization methods can be computed (see Table 4.3).

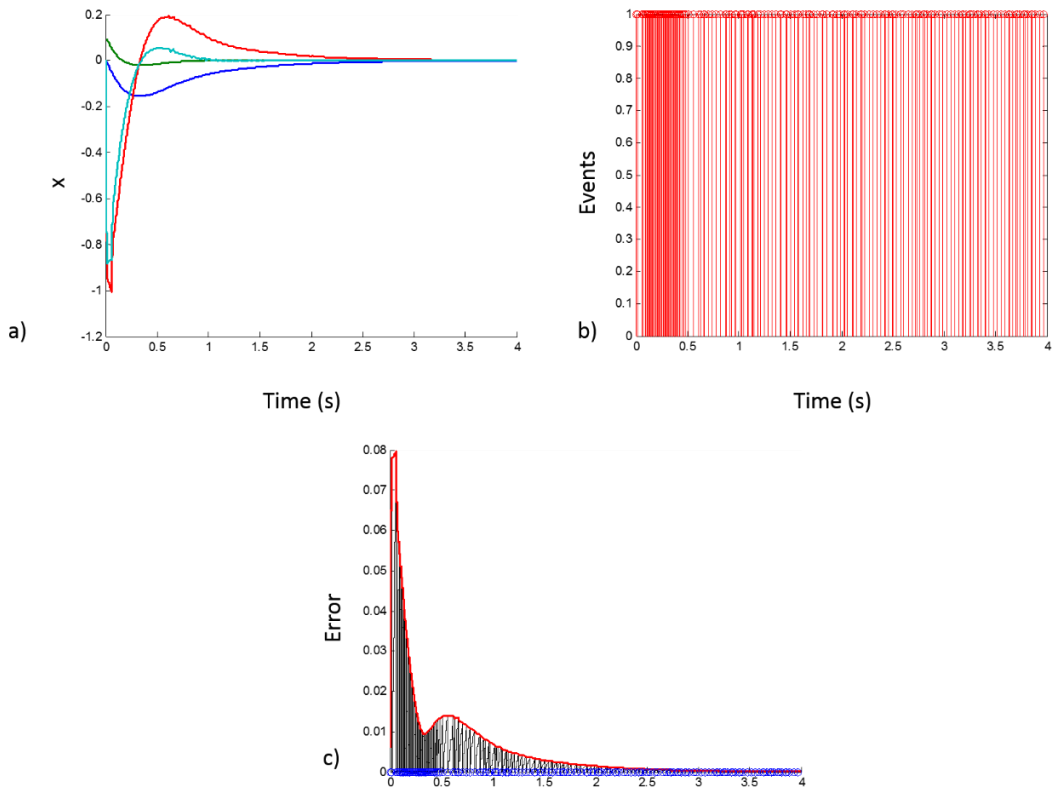

Figure 4.8: Simulation of the linear model of the RIP with gain K_{FZ}. In (a), the angle of the rotary arm is in blue, the angle of the pendulum in green, the angular velocity of the rotary arm in red and the angular velocity of the pendulum in cyan. In (b) each vertical line correspond to an event. (c) In black the evolution of the norm of the error. In red, the bound determined by the event condition (4.4)

It is easy to see that the maximum h is very small. This is caused because of the fast dynamics of the system. In fact, if we observe the difference in time between events in the ETC of the Figure 4.8c, the smallest time between two events is $2.18 \cdot 10^{-5}\ s$. It is important to remark that this h guarantees that the condition (4.4) never is violated but the system can be stabilized even if this condition does not always hold. An example can be seen in the Figure 4.9. The linear system is stabilized (a) but the event condition is violated in the intervals $0 - 0.007\ s$ and $0.06 - 0.065\ s$ (b).

Table 4.3: Comparison between the maximum h obtained for the different stabilization strategies which guarantee the stability.

Strategy	σ	Maximum h [s]
FSF	0.02	$8.09 \cdot 10^{-5}$
LQR	0.06	$2.68 \cdot 10^{-5}$
LQR based on TS	0.05	$3.68 \cdot 10^{-6}$

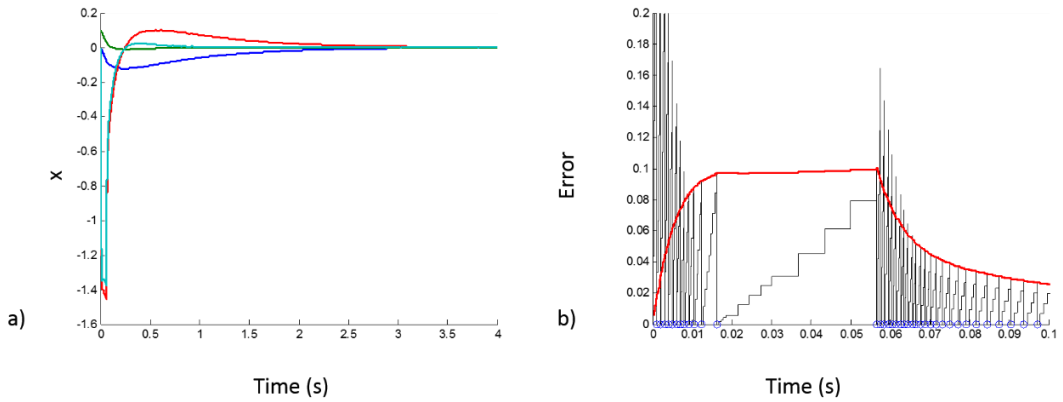

Figure 4.9: (a) Evolution of the states in the simulation of the RIP with gain K_{LQR}, $\sigma = 0.05$ and period $h = 0.001\ s$. (b) Violation of the bound (red) by the (error)

Since the sampling period for this RIP is $\sim 10\ ms$, it does not make sense to consider periods around $0.01\ ms$. This shows that the developed theorem for PETC yields conservative results that are unrealizable for systems as fast as the RIP.

5. SIMULATION PLATAFORM

5.1 Introduction

A simulator of the models has been deployed using a tool called Easy Java/Javascript Simulations [78]. The objective is to have a visual representation of the plants before the tests over the real plant. Moreover, it serves as a testing ground before to the implementation of new controllers or for educational purpose.

5.2 Easy Java/Javascript Simulations

Easy Java/Javascript Simulations (EjsS) is a free authoring tool written to create interactive simulations in an easy way. The principle advantages of EjsS are that it is free and open source software and that advanced knowledge in programming are not required in the creation of the simulations. In addition, EjsS gives high-level graphical capabilities as well as a high degree of interactivity and flexibility.

In this master thesis, a simulator for the RIP and the DRIP has been created using EjsS to show visually the dynamics of the plant and to allow tests of the different control laws.

More information about EjsS can be found at the site web: [79].

5.3 Simulation Description

The simulator deployed in EjsS allows the selection of:

- The dynamical model (RIP or DRIP)
- The stabilization controller (see Section 3)
- The sampling and control update strategy (see Section 0).

The current version of the simulator is based on a menus' system, so that the user can choose the simulator of the RIP or the DRIP. Then the user has the possibility to choose the type of the controller (FSF, LQR or Fuzzy for the RIP and LQR or an own controller for the DRIP). Besides, in the case of the RIP, it is available the decision of

the type of the control task update. This is made through the menus of a) in the Figure 5.1. The user has also the possibility to change the language (Spanish or English).

Once the user has selected a plant, the RIP by default, its view is shown (see Figure 5.1 for the RIP and Figure 5.3 for the DRIP). In the case of the RIP, the simulator has several panels that have been labelled from b) to f) (see Figure 5.1). In this case, we can display the linear model (red), the nonlinear model (blue) or both (panel b), so that the behaviours can be compared. Even more, both representations can be overlapped. Also a summary of the control design is shown in the panel c).

Moreover, the set-point for the angle motor can be change using a slider (see panel d)). Another slider allows the graphical overlapping commented above. On the right hand side, the different graphs show the positions, velocities, control signals in the panel e). Additional comments are given for the *Event* tab (see Figure 5.2). The graphs show a black curve that represents $\|e(t)\|$ and a red curve, which is the threshold. Also, the number of events, that is the number of samples and control task updates, is shown, as well as the number of times that the event condition is checked in both cases (linear and nonlinear).

The panel f) on the bottom right of the simulator, some numerical values are displayed. At the beginning of the simulation, it is possible to change them to define the initial conditions.

The simulator of the DRIP has a similar structure (see Figure 5.3). The graphical representation of the DRIP is shown in the panel a). Input commands to the motor angle can be given with the slider in the panel b), as in the case of the RIP. The main difference with the simulator of the RIP is that the user can introduce his own code and test it in the simulation (see panel c)). The use of this element will be explained later in the next subsection. On the right side, main variables of the model are represented in the panel d) and their values are shown in the panel e). As for the RIP, the initial conditions are chosen at the beginning of the simulation.

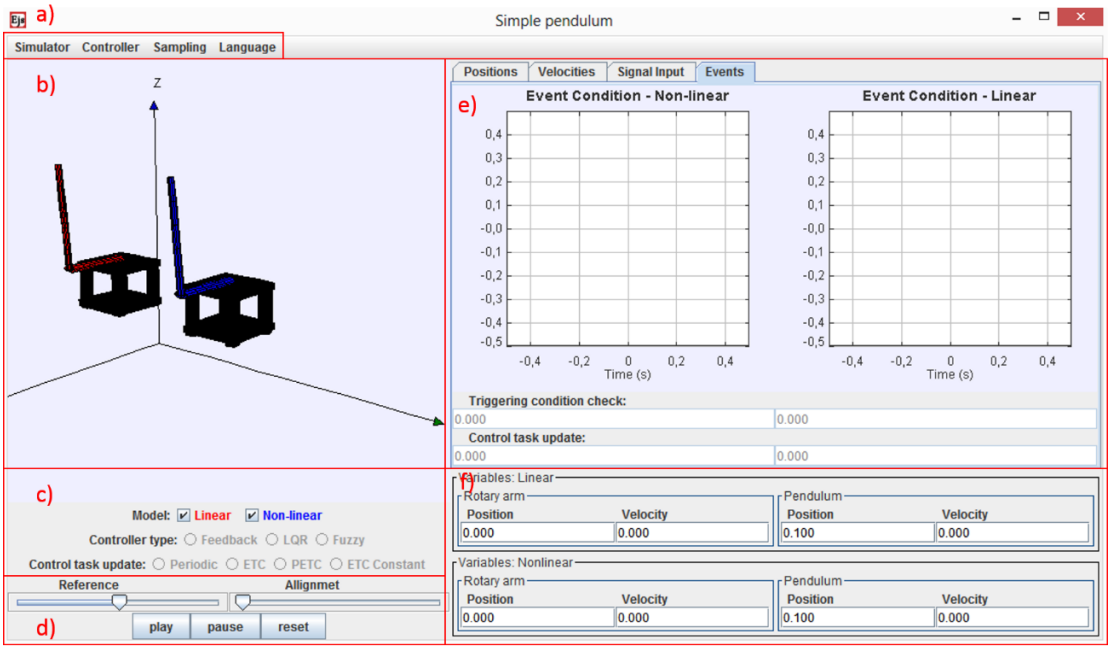

Figure 5.1: Scheme of the window of the simulator

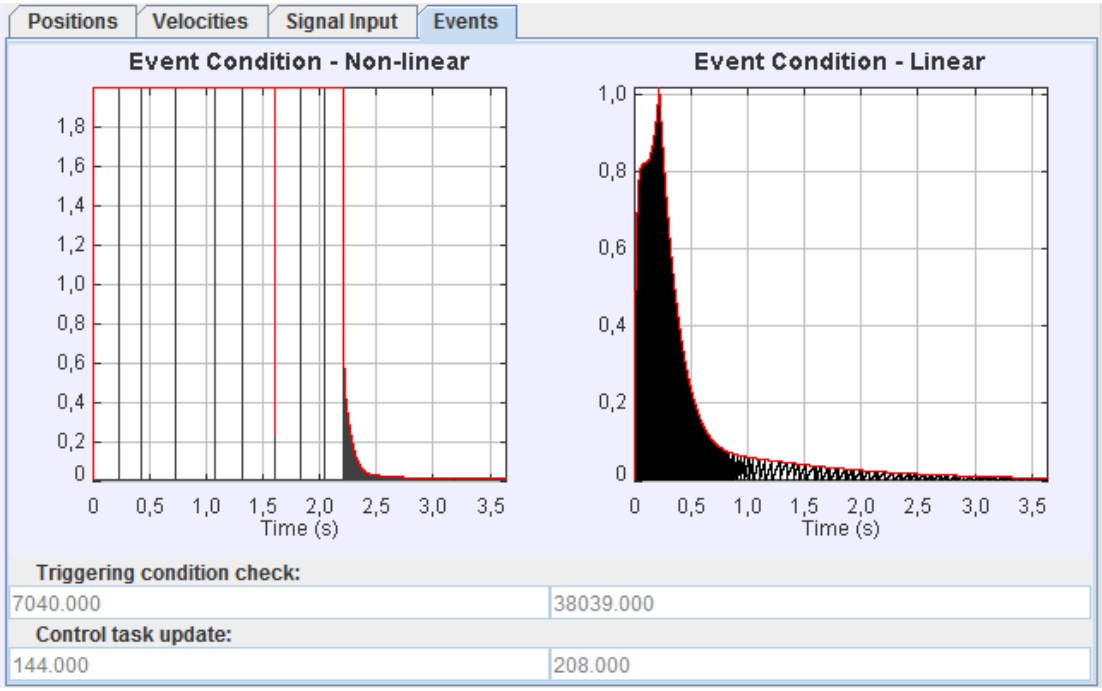

Figure 5.2: Event tab in the EjsS simulator of the RIP

5.4 Examples of Simulation and Use

In the simulator of the RIP, we can compare the linear and the nonlinear models. If the initial conditions are selected close to the upright position (equilibrium), the behaviour should be the same, as the Figure 5.4 shows.

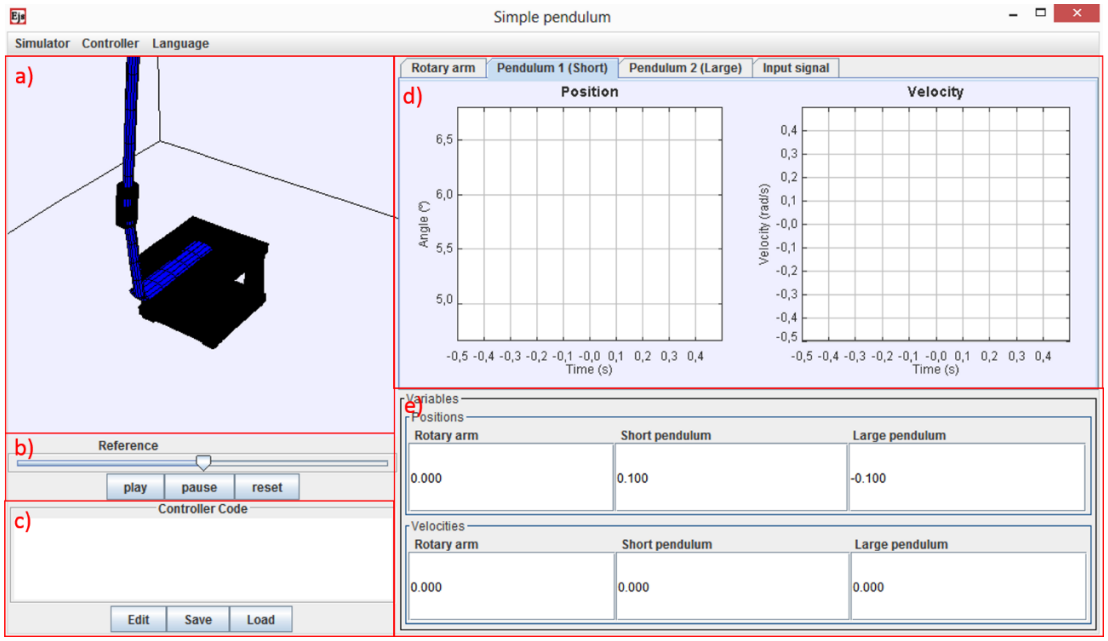

Figure 5.3: Simulator in EjsS of the double rotary inverted pendulum

The simulator allows to illustrate the influence of the design parameter σ. The higher σ is, the fewer events are triggered. In the Figure 5.5, these results are shown. Moreover, we can estimate which feedback gain requires more updates. We can see from the Table 5.1 that the control based on the Takagi-Sugeno model triggers less events to stabilize the RIP.

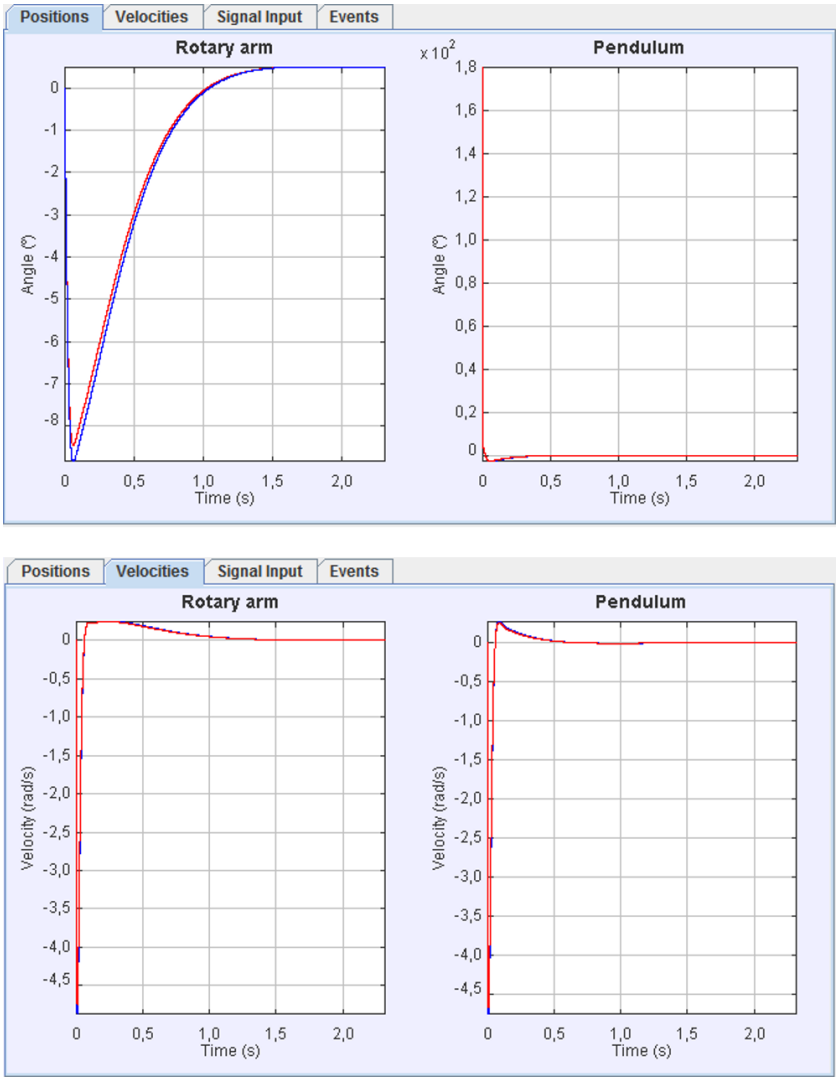

Figure 5.4: Simulation of the RIP with initial conditions $x_o^T = (0 \quad 0.1 \quad 0 \quad 0)$. The behaviour of the nonlinear model and the linear approximation are very close

Table 5.1: Number of events for the different controllers. $\sigma = 0.02$ and initial conditions $x_o^T = (0 \quad 0.1 \quad 0 \quad 0)$.

	FSF	LQR	TS
Events	733	632	615

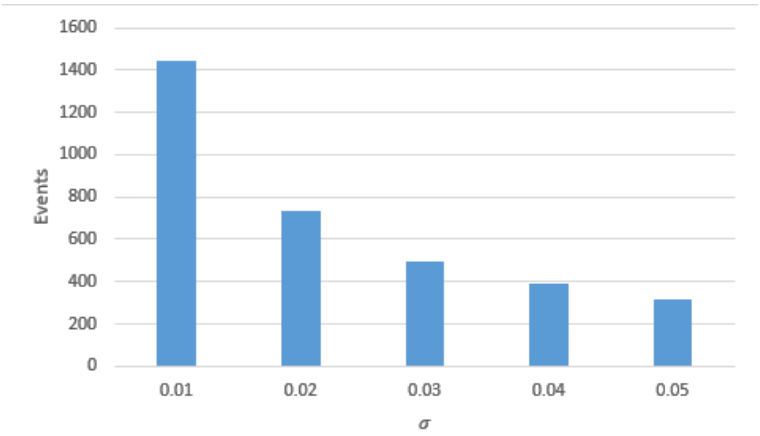

Figure 5.5: Number of events as a function of σ and for the LQR controller. Only the stabilization control is taken into account (initial conditions $x_o^T = (0 \quad 0.1 \quad 0 \quad 0)$)

Some properties of the event conditions can be easily observed. For example, the results for the event condition (4.4) are shown in the Figure 5.7a. On the contrary, the results when the event condition (4.5) is used are depicted in the Figure 5.7b. The simulation shows that when the constant event condition is used, the system is not asymptotically stable and the pendulum oscillates around the equilibrium point (see Figure 5.6).

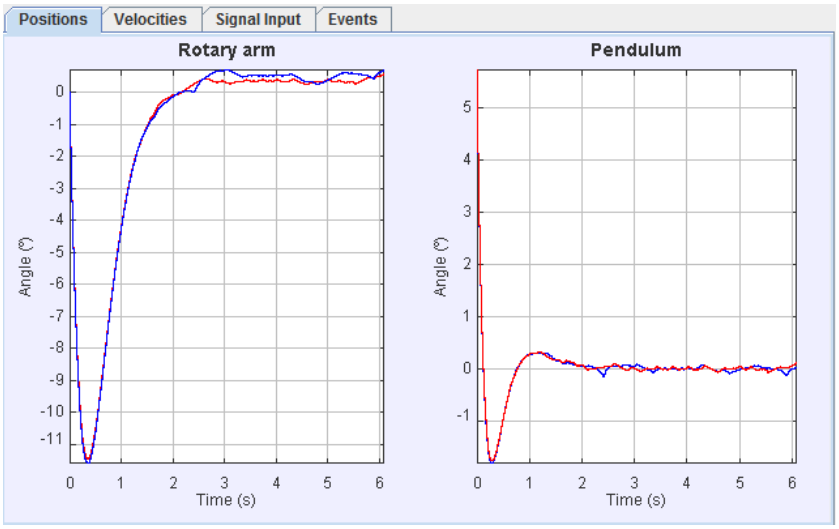

Figure 5.6: Simulation of the RIP using (4.5) with $c = 0.03$

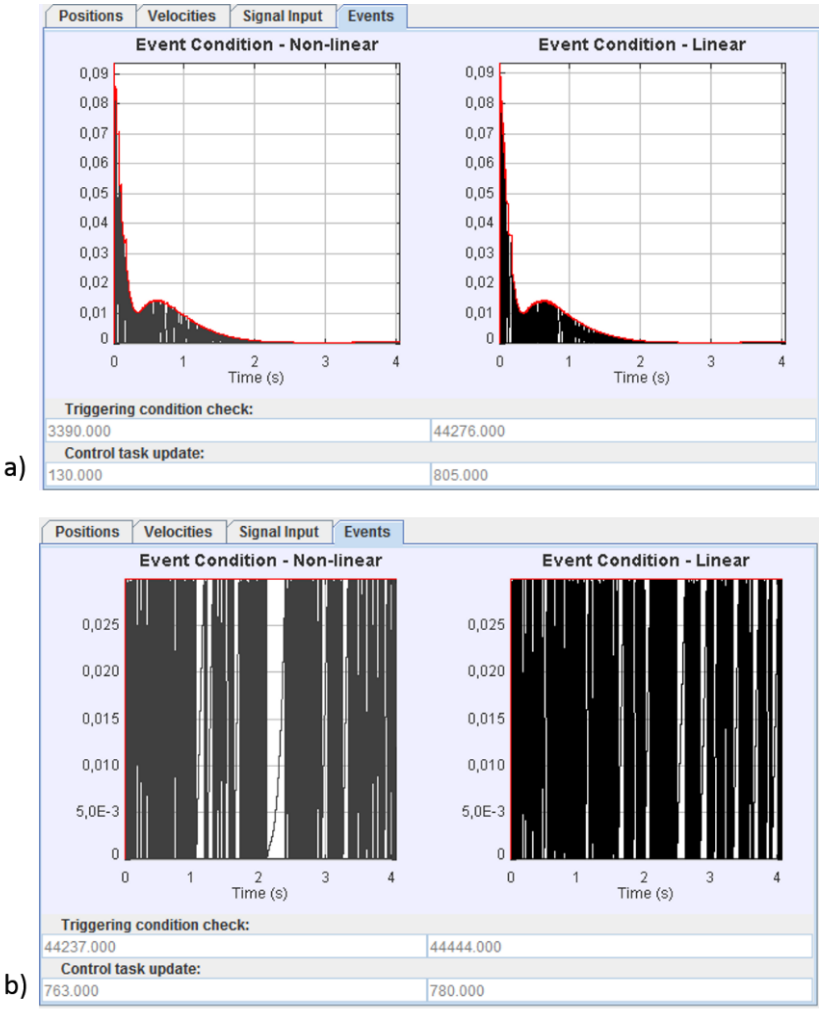

Figure 5.7: Comparison in simulation of the conditions (4.4) (a) and (4.5) (b)

The simulator of the DRIP can be used for two purposes. On one hand, the disturbances can be induced on the system clicking on the pendulum on the top. The magnitude of the disturbance will be proportional to the time that the user is clicking on it (see Figure 5.8). The user can see how the controller tries to reject the disturbance and the pendulum moves back to the equilibrium. If the disturbance cannot be rejected (Figure 5.8b), then the DRIP falls freely and describes a chaotic movement [80] until the friction stops it.

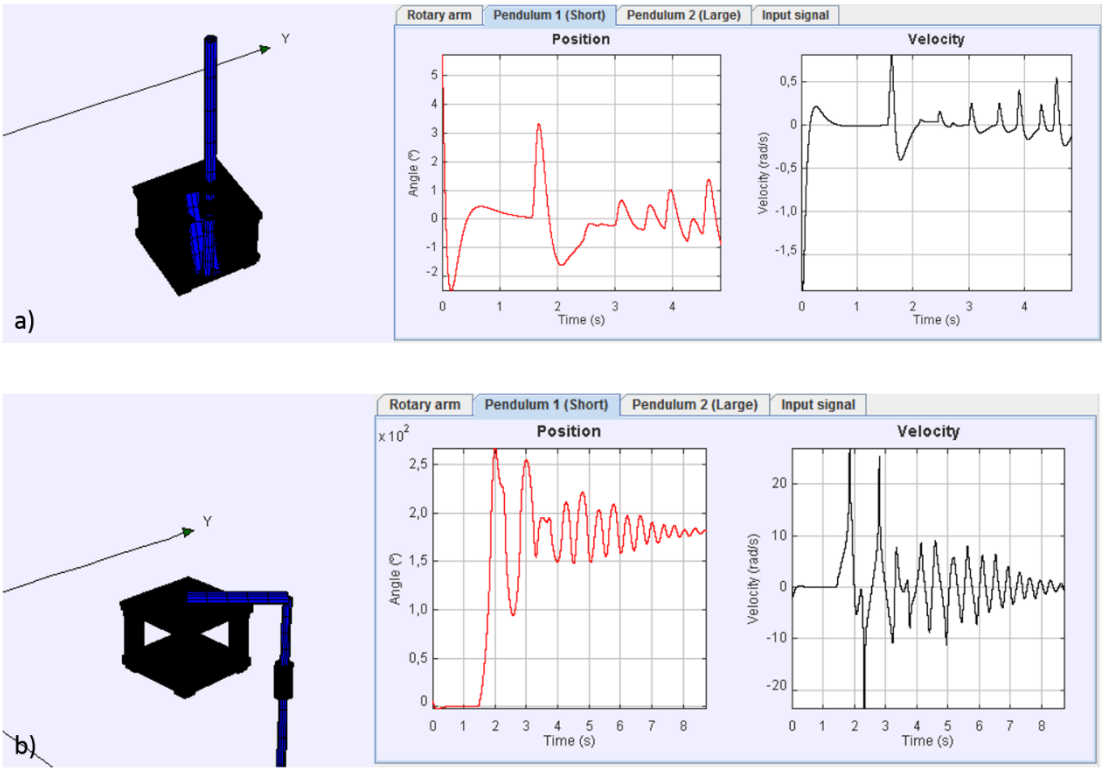

Figure 5.8: Behaviour of the DRIP to face a disturbances. In (a), small disturbances. In (b) an intense disturbances

On the other hand, the simulator of the DRIP includes an option to test controllers developed by the user. To do that, the user has to select *DRIP - Own controller* in the menu bar (see Figure 5.1a)). There are also three buttons: *edit*, *save* and *load*. If the user clicks on *edit*, a new window is displayed, where the user can write his own code. When the window is closed, the simulation starts using the written code as a controller. The buttons *save* and *load* allow to save and to get the controller codes to and from a txt file, respectively. In the Figure 5.9 we can see how the DRIP is stabilized using a simple controller implemented by the user.

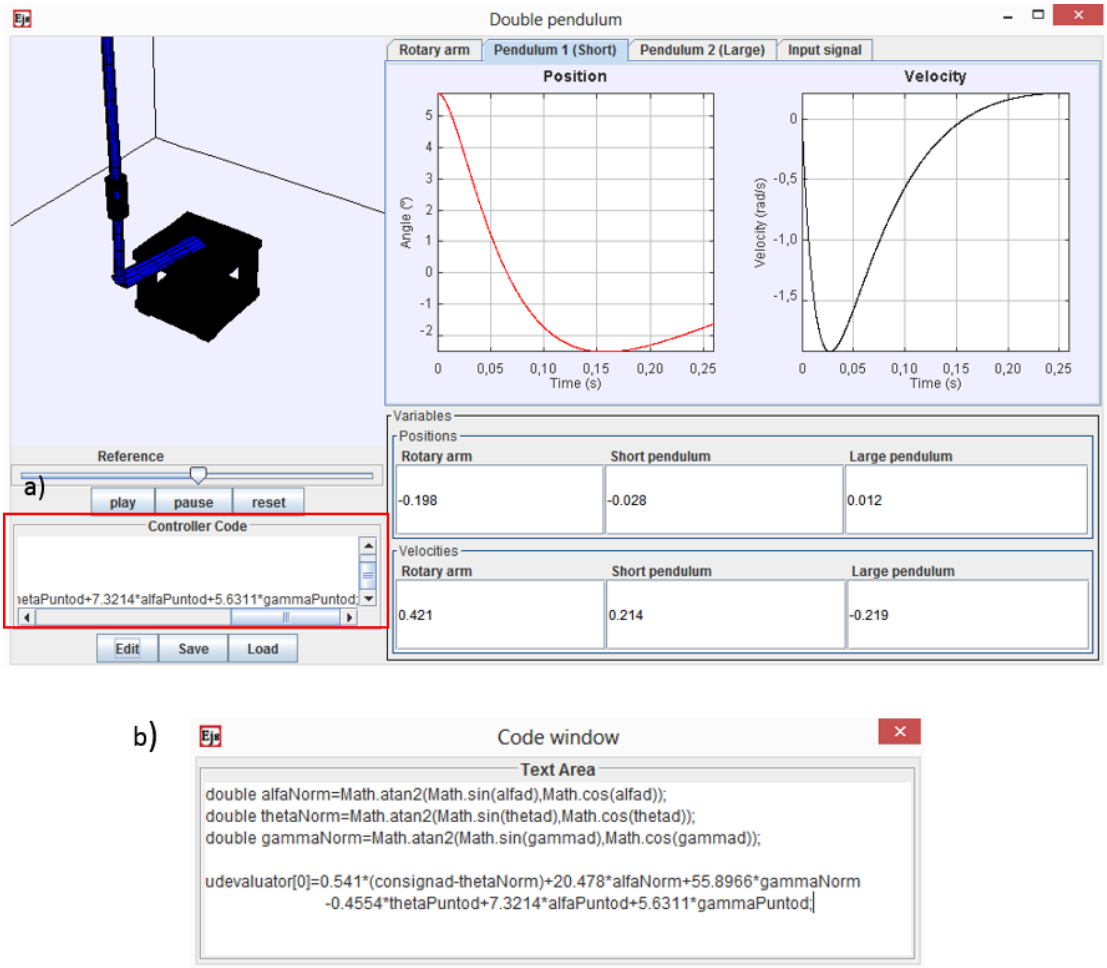

Figure 5.9: Control of the DRIP using a code written by the user. The red box (a) contains the written code. In (b), it can be seen enlarged

6. EXPERIMENTAL PLANT

6.1 Laboratory Description

The experimental plant consists of the RIP or DRIP of the Figure 1.3 attached to a SRV-02 gear (see Figure 6.1a). In the case of the RIP, two encoders measure the angles of the rotary arm and the pendulum. The encoders are connected to a data-acquisition board (see Figure 6.1b) which is also connected to the PC. In the case of the DRIP, an additional encoder is required to measure the angle of the second attached pendulum. A power amplifier (see Figure 6.1c) supplies the voltage to the motor.

Figure 6.1: (a) SRV-02 motor, (b) Q8-USB data-acquisition board, (c) VoltPAQ-XI power amplifier from Quanser Inc.

6.2 Experimental Results for the RIP

In the case of the RIP, two experiments have been performed to study: i) The region of attraction of the different stabilization controllers, ii) The events triggered in the different sampling strategies.

For the first experiment, the regions of attraction for the different controllers are shown in the Table 6.1. As we predicted with the simulations of the Subsection 3.2.2, the region of attraction of the controller based on a model of Takagi-Sugeno is the largest. However, the results are not as significantly different as in the simulation (see Table 3.2). The cause of this might be model uncertainties.

Table 6.1: Comparison of the maximum region of attraction of the different stabilization control strategies for the RIP in the experimental lab.

Strategy	Maximum region of attraction	Improvement of LQR based on TS
FSF	±31.5°	27.6%
LQR	±34.3°	17.2%
LQR based on TS	±40.2°	-

The evolution of the states is shown below. The angles described by the rotary arm and by the pendulum for the three controllers are represented in the Figure 6.2 and the Figure 6.3, respectively. The corresponding velocities are shown in the Figure 6.4 and the Figure 6.5. In the Figure 6.6, the input signal is displayed. If the results are compared, we conclude that the maximum region of attraction for the stabilization is larger in the fuzzy control and, moreover, this stabilization is achieved in less time than in the FSF control or the LQR control.

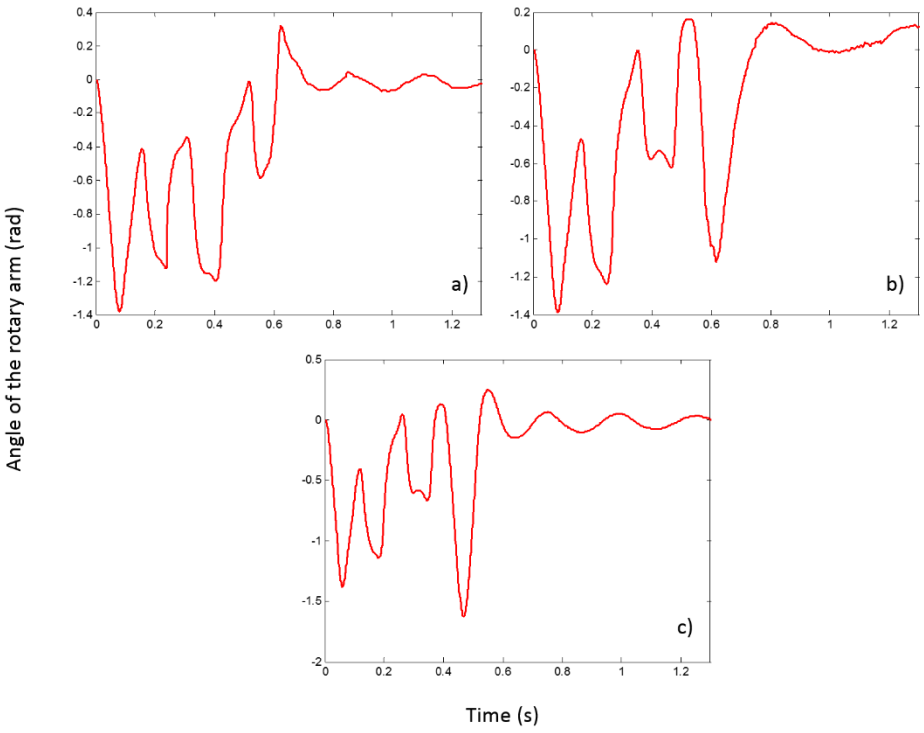

Figure 6.2:Measurement of the angle described by the rotary arm in the case of a) FSF control with switch from swing-up to stabilization in $\alpha = 31.5°$, b) LQR control with switch from swing-up to stabilization in $\alpha = 34.3°$ and c) LQR control based on a fuzzy model of TS with switch from swing-up to stabilization in $\alpha = 40.2°$

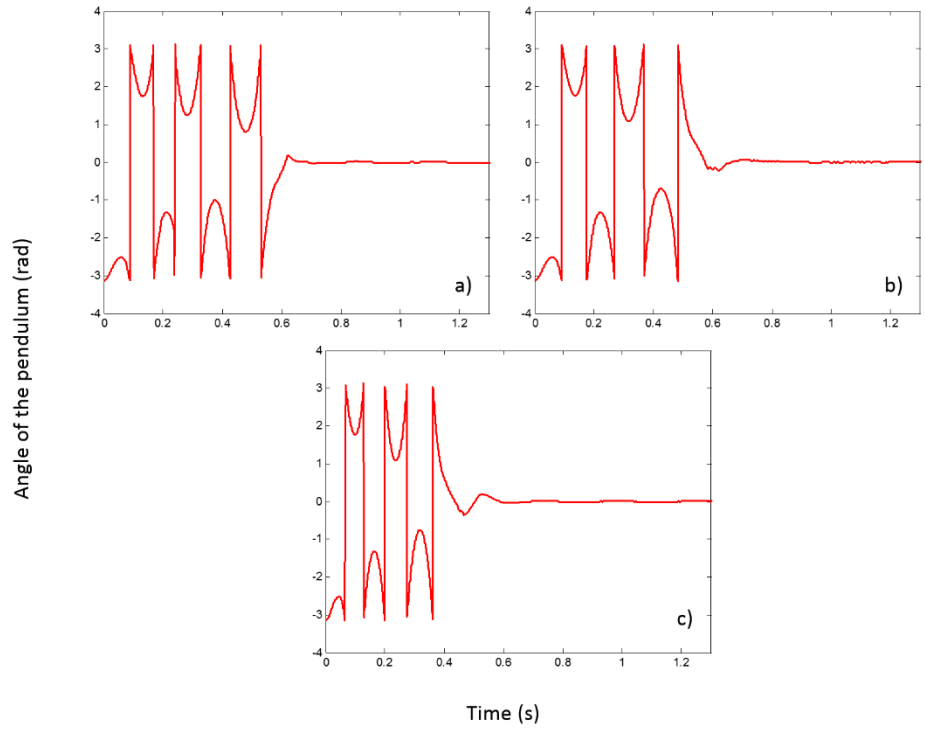

Figure 6.3: Measurement of the angle described by the pendulum in the case of a) FSF control with switch from swing-up to stabilization in $\alpha = 31.5°$, b) LQR control with switch from swing-up to stabilization in $\alpha = 34.3°$ and c) LQR control based on a fuzzy model of TS with switch from swing-up to stabilization in $\alpha = 40.2°$

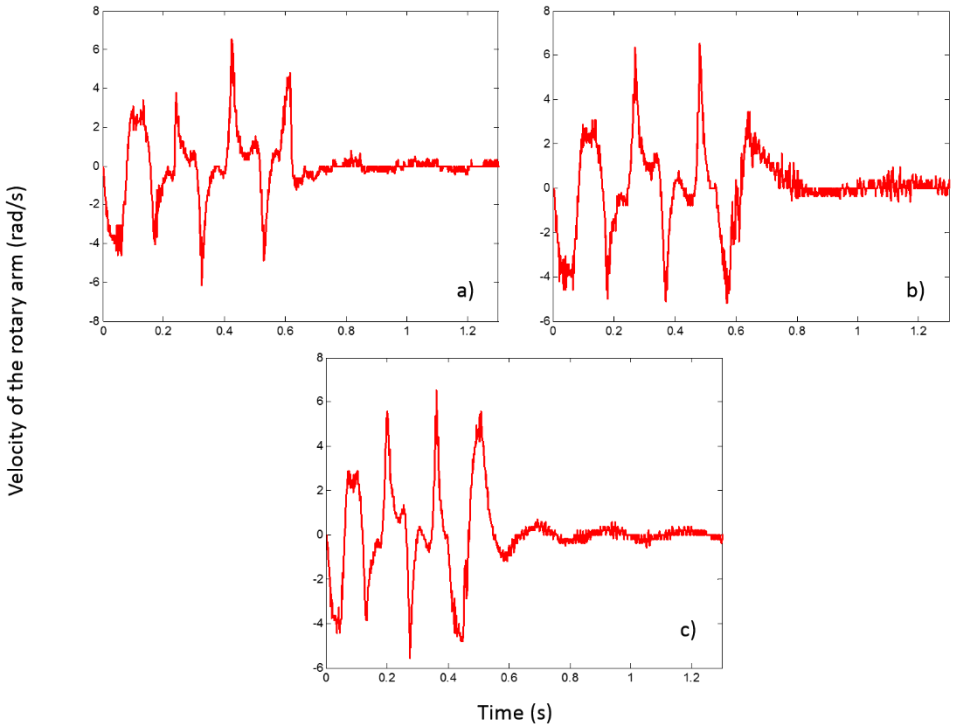

Figure 6.4: Measurement of the velocity of the rotary arm in the case of a) FSF control with switch from swing-up to stabilization in $\alpha = 31.5°$, b) LQR control with switch from swing-up to stabilization in $\alpha = 34.3°$ and c) LQR control based on a fuzzy model of TS with switch from swing-up to stabilization in $\alpha = 40.2°$

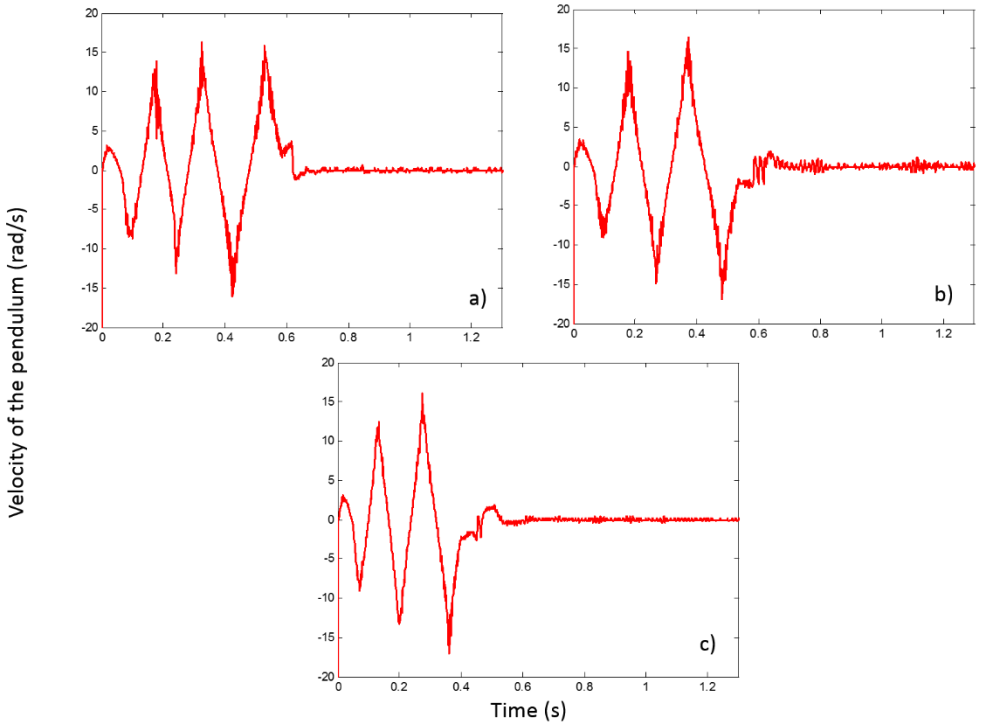

Figure 6.5: Measurement of the velocity of the pendulum in the case of a) FSF control with switch from swing-up to stabilization in $\alpha = 31.5°$, b) LQR control with switch from swing-up to stabilization in $\alpha = 34.3°$ and c) LQR control based on a fuzzy model of TS with switch from swing-up to stabilization in $\alpha = 40.2°$

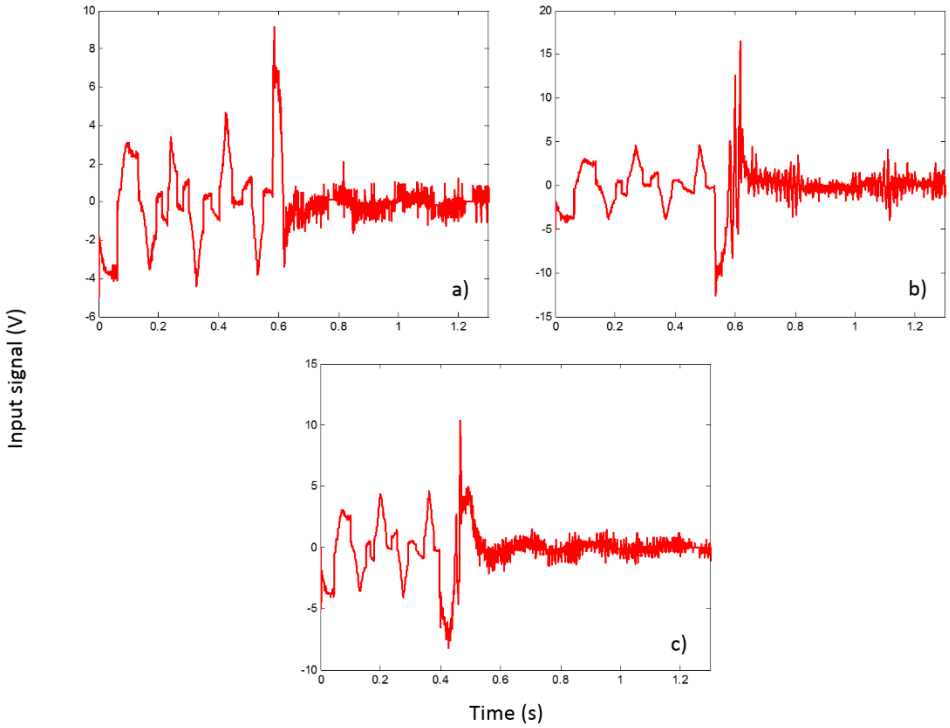

Figure 6.6: Measurement of the input signal in the case of a) FSF control with switch from swing-up to stabilization in $\alpha = 31.5°$, b) LQR control with switch from swing-up to stabilization in $\alpha = 34.3°$ and c) LQR control based on a fuzzy model of TS with switch from swing-up to stabilization in $\alpha = 40.2°$

As far as the event triggering design is concerned, the theoretical bound of the sampling period obtained for the PETC in the subsection 4.5 is too small to be implemented in an experimental lab. Nevertheless, we can test the results. In the Table 6.2 we can see a comparison of the number of events produced in $15\ s$ using the TDC and using PETC with a sampling period of $h = 10\ ms$.

Table 6.2: Comparison between TDC and PETC in the experimental plant.

Strategy	Events in the TDC	σ	Events in the PETC	Reduction
FSF	1090	0.03	784	28.1%
LQR	1096	0.1	800	27.0%
LQR based on TS	1010	0.2	674	33.3%

We can plot the evolution of the states in the last case (TS model) as an example (see Figure 6.7). We observe how the behaviour is very similar to the one obtained with the periodic control (Figure 6.2 - Figure 6.6). The number of events have been clearly reduced and hence, the waste of communication resources. However, it is not guaranteed that the event condition holds for such a large h. In fact, taking a look to the Figure 6.8, we check that the threshold is exceeded several times.

If we compare the results of the Table 6.2 with the Table 4.2 of the Section 4.5, the order of the reduction of updates is similar in the case of LQR and TS ($\sim 30\%$).

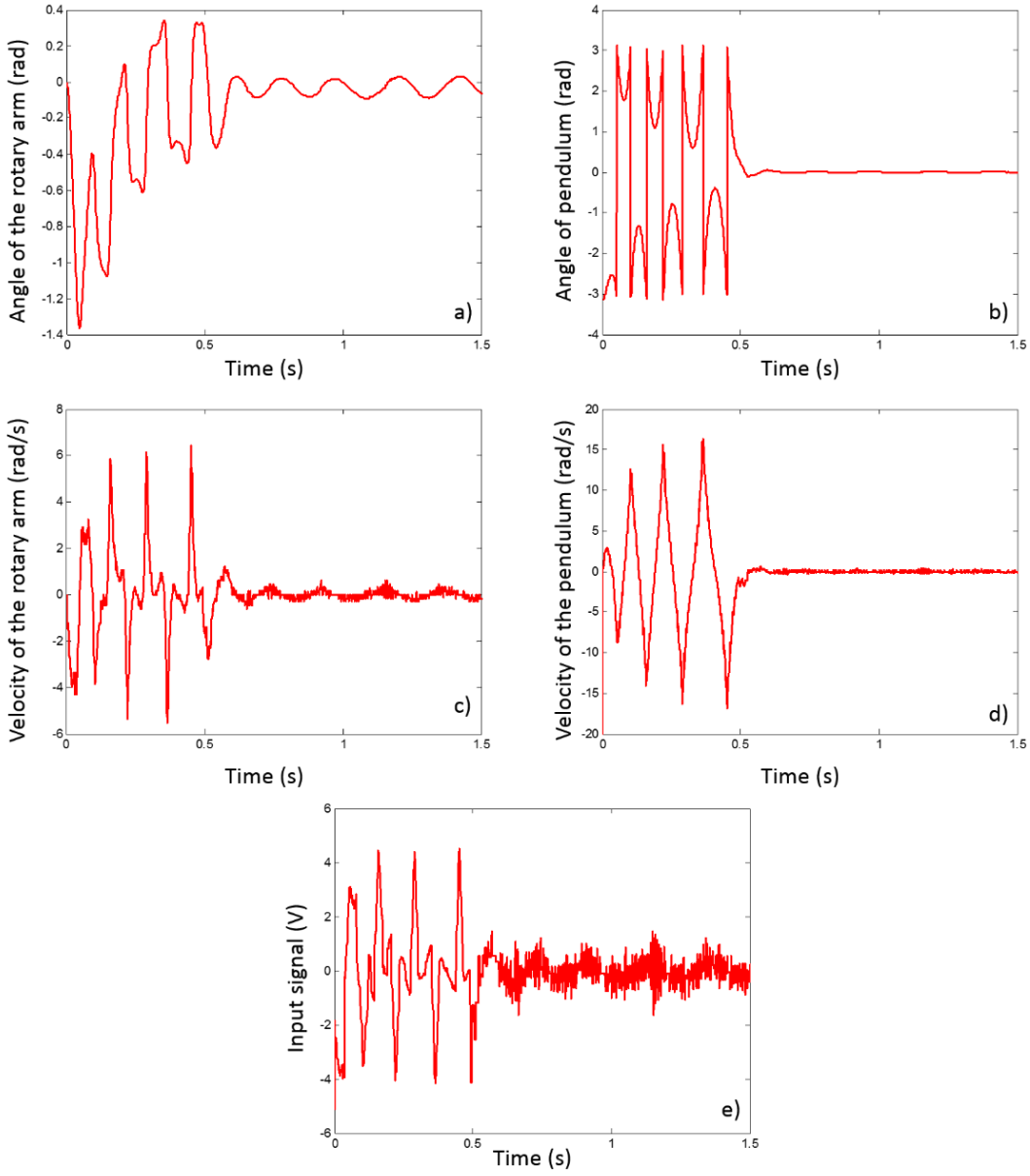

Figure 6.7: Evolution of the states using the TS control and the PETC. a) Angle described by the rotary arm. b) Angle described by the pendulum. c) Velocity of the rotary arm. d) Velocity of the pendulum. e) Input signal.

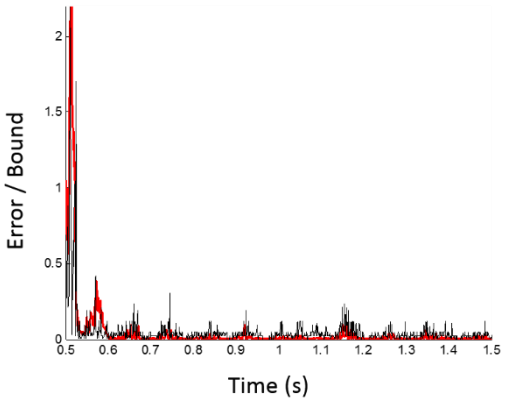

Figure 6.8: The evolution of the error (black) and the bound (red) with the fuzzy control in the case of the PETC in the experimental plant

6.3 Experimental Results for the DRIP

In the case of the DRIP, the plant can serve to test the computed feedback gain and how it responses to disturbances. The evolution of the states and the inputs signal are presented in the Figures 6.9 – 6.11. We can observe that the computed feedback gain keeps the DRIP in the unstable equilibrium position.

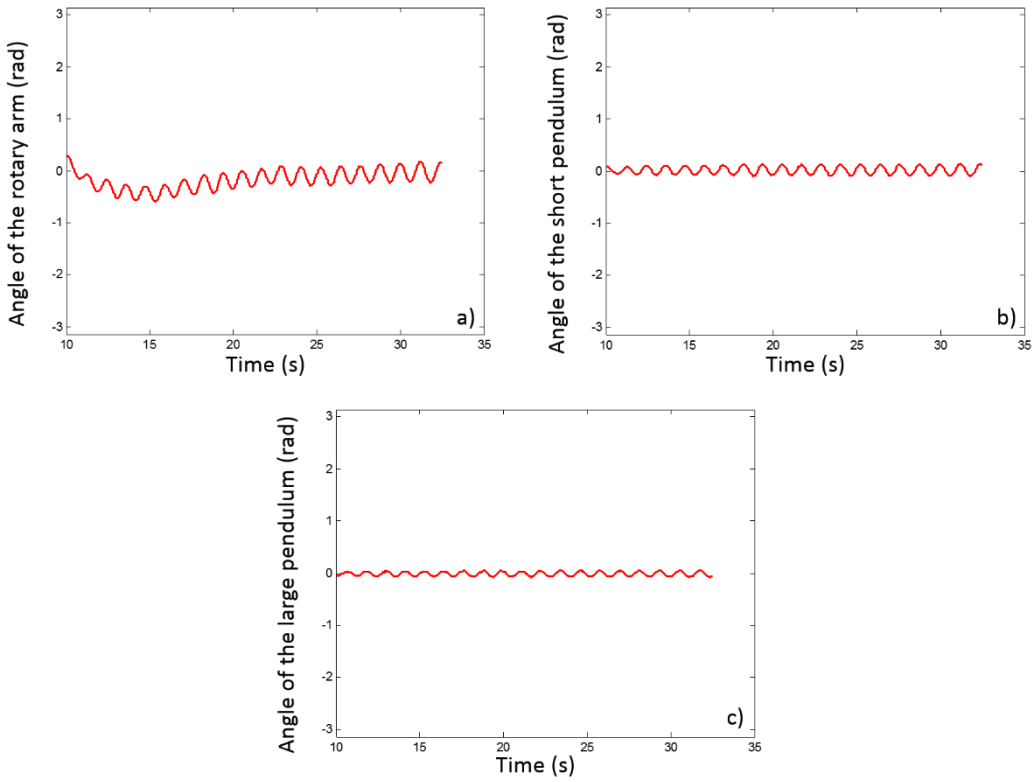

Figure 6.9: Measurement of the angles described by the rotary arm (a) and the pendulums (b-c) while its stabilization

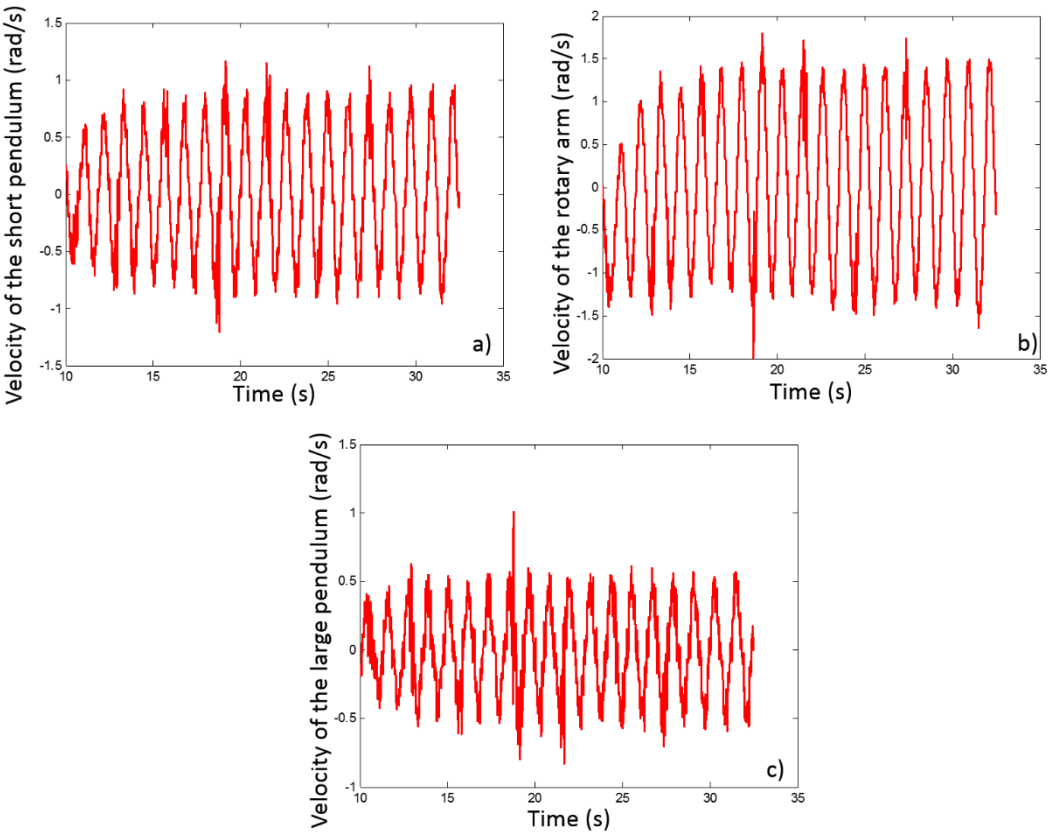

Figure 6.10: Measurement of the velocities of the rotary arm (a) and the pendulums (b-c) while its stabilization

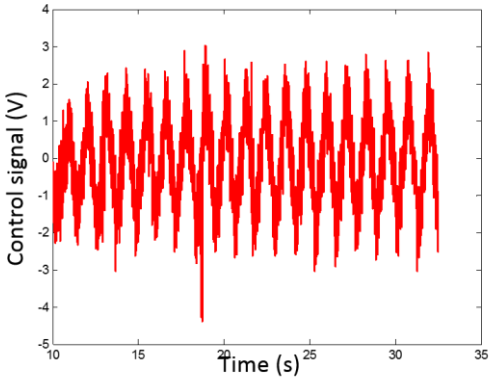

Figure 6.11: Measurement of the input signal while the stabilization of the DRIP

7. CONCLUSIONS AND FUTURE WORK

7.1 Conclusions

This master thesis has studied the dynamical models of the RIP and DRIP as well as different control and sampling strategies. A simulation tool developed in EjsS to evaluate different control designs has been presented. Finally, the experimental results have illustrated the results. Hence, the conclusions deduced from this master thesis can be structured as follows.

First, the region of attraction of the rotary inverted pendulum has been studied. A new feedback gain has been derived from a fuzzy model of Takagi-Sugeno. This feedback gain has been tested in the real plant with best results than in the case of classical controllers as FSF and LQR. Specifically, it improves 27.6% respect to FSF and 17.2% respect to the LQR.

To reduce the waste of resources, different ways to sample and update the control task have been studied. The classical time-driven control has been compared with the event-triggered control. Moreover, the periodic event-triggered control, a combination of both, has been considered. The objective is to reduce the waste of communication resources (as in ETC) and the waste of computation resources (as in TDC). In this direction, the Theorem 4.2 has been proposed. It provides a period h which guarantees that, if the event condition is checked only at multiples of h, then the system is asymptotically stable and the event condition is never violated in the interval $(nh, (n+1)h)$.

These strategies for the control task update have been applied to the rotary inverted pendulum. This system has several difficulties due to its fast dynamics. However, the simulation results have shown that the ETC provides an important reduction in the number of updates for the case of the LQR (36.75%) and the TS (27.75%). The application of the Theorem 4.2 to the RIP provides very small periods, that makes this design non-implementable in the experimental plant. The reason for this is that the event condition can be violated in short periods of time due to the fast

dynamics. However, for a system with slower dynamics (a DC motor) the usefulness of the PETC has been clearly demonstrated

The event-based control has been successfully implemented in the experimental plant, yielding a considerable reduction of control task updates (approximately 30%), even though the event condition is violated several times.

Some preliminary results have been obtained for the DRIP. The dynamical model and the study of the stabilization controller have been presented.

As final contribution of this master thesis, a simulator in EjsS has been developed for the RIP and the DRIP. The objective is to provide an intuitive, interactive, graphical simulation, which provides the users an insight of the hands-on lab. In addition, it serves as a starting point to include this plant in the network of remote labs the department coordinates.

7.2 Future Work

Some of the future work can be deduced from the previous conclusions. On the one hand, the improvement of the Theorem 4.2 which yields a conservative choice of the sampling period can be tackled by the use of Lyapunov functionals, because the bound to $\dot{V}$ results less conservative [81]. Another line of research can be the design of more appropriately event conditions. Both directions could make implementable the formalism of ETC and PETC in plants with fast and unstable dynamics, such as the RIP.

On the other hand, a complete study of the DRIP is still a long way away. It is necessary to improve the region of attraction of stabilization to develop an effective swing-up control law. This may be done using the fuzzy strategy proposed.

Finally, as we have mentioned, the integration of the plant in the network of remote laboratories Unilabs [82] should be a fundamental objective.

References

[1] K. Furuta, M. Yamakita and S. Kobayashi, “Swing-up Control of Inverted Pendulum Using Pseudo-State Feedback,” *Journal of Systems and Control,* vol. 206, no. 4, pp. 263-269, 1992.

[2] K. Astrom and K. Furuta, “Swinging up a Pendulum by Energy Control,” *Automatica,* vol. 36, no. 2, pp. 287-295, 2000.

[3] F. Leung, L. Wong and P. Tam, “Fuzzy Model Based Controller for an Inverted Pendulum,” *Electronics Letters,* vol. 32, no. 18, p. 1683 – 1685, 1996.

[4] J. Zhao and M. Spong, “Hybrid Control for Global Stabilization of the Cart-Pendulum System,” *Automatica,* vol. 37, no. 12, pp. 1941-1951, 2001.

[5] N. Muskinja and B. Tovornik, “Swinging Up and Stabilization of a Real Inverted Pendulum,” *IEEE Transactions on Industrial Electronics,* vol. 53, no. 2, pp. 631-639, 2006.

[6] H. Vargas, J. Sanchez Moreno, C. Jara, F. Candelas, F. Torres and S. Dormido, “A Network of Automatic Control Web-Based Laboratories,” *IEEE Transactions Learning Technologies,* vol. 4, no. 3, pp. 197-208, 2011.

[7] M. Guinaldo, “Contributions to Networked and Event-Triggered Control of Linear Systems,” PhD Thesis, Universidad Nacional de Eduacion a Distancia, 2013.

[8] J. Lunze and D. Lehmann, “A State-Feedback Approach to Event-Based Control,” *Automatica,* vol. 46, no. 1, pp. 211-215, 2010.

[9] P. Tabuada, “Event-Triggered Real-Time Scheduling of Stabilizing Control Tasks,” *Transactions on Automatic Control,* vol. 52, no. 9, pp. 1680-1685, 2007.

[10] W. Heemels, M. Donkers and A. Teel, “Periodic Event-Triggered Control for Linear Systems,” *Transactions on Automatic Control,* vol. 58, no. 4, pp. 847-861, 2013.

[11] S. Dormido, J. Sánchez and E. Kofman, “Muestreo, Control y Comunicación basados en Eventos (In Spanish),” *Revista Iberoamericana de Automática e Informática Industrial,* vol. 5, no. 1, pp. 5-26, 2008.

[12] N. Kouda, N. Matsui and H. Nishimura, “Control for Swing-up of an Inverted Pendulum using Qubit Neural Network,” in *Proceedings of the 41th SICE Annual Conference*, 2002.

[13] C. Anderson, “Learning to Control an Inverted Pendulum using Neural Networks,” *IEEE Control Systems Magazine,* vol. 9, no. 3, pp. 31-37, 1989.

[14] N. Bhattathiri and P. Saraswathi, “ANN Control of Non-Linear and Unstable System and its Implementation on Inverted Pendulum,” *International Journal of Current Engineering and Technology,* vol. 4, no. 2, pp. 826-831, 2014.

[15] C. Ji, F. Lei and L. Kin, “Fuzzy Logic Controller for an Inverted Pendulum System,” in *IEEE International Conference on Intelligent Processing Systems*, 1997.

[16] P. Mohanlal and M. Kaimal, “Exact Fuzzy Modeling and Optimal Control of the Inverted Pendulum on Cart,” in *IEEE Conference on Decision and Control*, 2002.

[17] R. Harrison, “Asymptotically Optimal Stabilising Quadratic Control of an Inverted Pendulum,” *IEE Proceedings - Control Theory and Applications,* vol. 150, no. 1, pp. 7-16, 2003.

[18] H. Lam, F. Leung and P. Tam, “Design and Stability Analysis of Fuzzy Model based Nonlinear Controller for Nonlinear Systems using Genetic Algorithm,” in *IEEE International Conference on Fuzzy Systems*, 2002.

[19] K. Pathak, J. Franch and S. Agrawal, “Velocity and Position Control of a Wheeled Inverted Pendulum by Partial Feedback Linearization,” *IEEE Transactions on Robotics,* vol. 21, no. 3, pp. 505-513, 2005.

[20] K. Åström, J. Aracil and F. Gordillo, “A Family of Smooth Controllers for Swinging up a Pendulum,” *Automatica,* vol. 44, no. 7, pp. 1841-1848, 2008.

[21] M. Park and D. Chwa, “Swing-Up and Stabilization Control of Inverted-Pendulum Systems via Coupled Sliding-Mode Control Method,” *IEEE Transactions on Industrial Electronics,* vol. 56, no. 9, pp. 3541-3555, 2009.

[22] J. Wang, “Simulation Studies of Inverted Pendulum based on PID Controllers,” *Simulation Modelling Practice and Theory,* vol. 19, no. 1, pp. 440-449, 2011.

[23] F. Mazenc and L. Praly, “Asymptotic Tracking of a Reference State for Systems with a Feedforward Structure,” *Automatica,* vol. 36, no. 2, pp. 179-187, 2000.

[24] A. Mills, A. Wills and B. Ninness, “Nonlinear Model Predictive Control of an Inverted Pendulum,” in *American Control Conference*, 2009.

[25] O. Boubaker, “The inverted Pendulum Benchmark in Nonlinear Control Theory: A Survey,” *International Journal of Advanced Robotic Systems,* no. 10, pp. 233-242, 2013.

[26] J. Aracil and F. Gordillo, “The Inverted Pendulum: a Benchmark in Nonlinear Control,” in *Automation Congress*, 2004.

[27] P. Ponce, A. Molina and E. Alvarez, “A Review of Intelligent Control Systems Applied to the Inverted-Pendulum Problem,” *American Journal of Engineering and Applied Sciences,* vol. 7, no. 2, pp. 161-207, 2014.

[28] P. Ellis, “Extension of Phase Plane Analysis to Quantized Systems,” *IRE Transactions on Automatic Control,* vol. 4, no. 2, pp. 43-54, 1959.

[29] K. Årzén, “A Simple Event-Based PID Controller,” in *IFAC World Congress* , 1999.

[30] W. Heemels, R. Gorter, A. van Zijl, P. van den Bosch, S. Weiland, W. Hendrix and M. Vonder, “Asynchronous Measurment and Control: a Case Study on Motor synchronization,” *Control Engineering Practice,* vol. 7, no. 12, pp. 1467-1482, 1999.

[31] X. Wang and M. Lemmon, “Event Design in Event-Triggered Feedback Control Systems,” in *IEEE Conference on Decision and Control*, 2008.

[32] X. Wang and M. Lemmon, “On Event Design in Event-Triggered Feedback Systems,” *Automatica,* vol. 47, no. 10, p. 2319–2322, 2011.

[33] E. García and P. Antsaklis, “Model-Based Event-Triggered Control with Time-Varying Network Delays,” in *Conference on Decision and Control and European Control*, 2011.

[34] W. Heemels and M. Donkers, “Model-Based Periodic Event-Triggered Control for Linear Systems,” *Automatica,* vol. 49, no. 3, pp. 698-711, 2013.

[35] E. García and P. Antsaklis, “Model-Based Event-Triggered Control for Systems with Quantization and Time-Varying Network Delays,” *IEEE Transactions on Automatic Control,* vol. 58, no. 2, pp. 422-434, 2013.

[36] R. Postoyan, A. Anta, W. Heemels, P. Tabuada and D. Nesic, “Periodic Event-Triggered Control for Nonlinear Systems,” in *IEEE Conference on Decision and Control*, 2013.

[37] D. Yue, E. Tian and Q. Han, “A Delay System Method for Designing Event-Triggered Controllers of Networked Control Systems,” *IEEE Transactions on Automatic Control,* vol. 58, no. 2, pp. 475-481, 2013.

[38] S. Hu and D. Yue, “Event-Triggered Control Design of Linear Networked Systems with Quantizations,” *ISA Transactions,* vol. 51, no. 1, pp. 153-162, 2012.

[39] W. Heemels, J. Sandee and P. Van den Bosch, “Analysis of Event-Driven Controllers for Linear Systems,” *International Journal of control,* vol. 81, no. 4, pp. 571-590, 2008.

[40] M. Mazo, A. Anta and P. Tabuada, “On Self-Triggered Control for Linear Systems: Guarantees and Complexity,” in *IEEE European Control Conference*, 2009.

[41] X. Wang and M. Lemmon, “Self-Triggered Feedback Control Systems with Finite Gain L_2 Stability,” *IEEE Transactions on Automatic Control,* vol. 53, no. 3, pp. 452-467, 2009.

[42] M. Velasco, P. Martí and J. Fuertes, “The Self-Triggered Task Model for Real-Time Control Systems,” in *IEEE Real-Time Systems Simposium*, 2003.

[43] A. Anta and T. P., “On the Minimum Attention and Anytime Attention Problems for Nonlinear Systems,” in *IEEE Conference on Decision and Control*, 2010.

[44] M. Donkers, P. Tabuada and W. Heemels, “Minimum Attention Control for Linear Systems: A Linear Programming Approach,” in *Discrete Event Dynamic Systems Theory and Applications*, 2012.

[45] Q. Liu, Z. Wang and D. Zhou, “A Survey of Event-Based Strategies on Control and Estimation,” *Systems Science & Control Engineering,* vol. 4, no. 1, pp. 90-97, 2014.

[46] S. Durand, J. Guerrero Castellanos, N. Marchand and W. Guerrero Sanchez, “Event-Based Control of the Inverted Pendulum: Swing up and Stabilization,” *Journal of Control Engineering and Applied Informatics,* vol. 15, no. 3, pp. 96-104, 2013.

[47] H. Goldstein, C. Poole and J. Safko, Classical Mechanics (3rd Edition), Addison Wesley, 2001.

[48] B. Brunt, The Calculus of Variations, Springer, 2004.

[49] A. Stephenson, “A New Type of Dynamic Stability,” *Memoirs and Proceedings of the Manchester Literary and Philosophical Society,* vol. 52, no. 8, pp. 1-10, 1908.

[50] A. Castro, “Modeling and dynamic analysis of a two-wheeled inverted pendulum,” Master Thesis, Georgia Institute of Technology, 2012.

[51] J. Aracil and F. Gordillo, “El Péndulo Invertido: un Desafío para el Control no Lineal (in Spanish),” *Revista Iberoamericana de Automática e Informática Industrial,* vol. 2, no. 2, pp. 8-19, 2005.

[52] T. Sugihara, Y. Nakamura and H. Inoue, “Real-Time Humanoid Motion Generation through ZMP Manipulation based on Inverted Pendulum Control,” in *International Conference on Robotics and Automation*, 2002.

[53] K. Tamaki, K. Suyehiro, J. Allan and M. McWilliams, “Broadband Downhole Digital Seismometer Experiment at Site 794: a Technical Paper,” *Proceedings of the Ocean Drilling Program,* vol. 127, no. 2, 1992.

[54] D. Rosen, “Harmonic Metronome”. USA Patent US5515764 A, 1996.

[55] S. Jadlovská and J. Sarnovský, “Modelling of Classical and Rotary Inverted Pendulum Systems – a Generalized Approach,” *Journal of Electrical Engineering,* vol. 64, no. 1, pp. 12-19, 2013.

[56] M. Fairus, Z. Mohamed and N. Ahmad, “Fuzzy Modeling and Control of Rotary Inverted Pendulum System using LQR Technique,” in *5th International Conference on Mechatronics*, 2013.

[57] H. K. Khalil, “Lyapunov Stability,” in *Nonlinear Systems Third Edition*, New Jersey, Prentice Hall, 2002, pp. 111-181.

[58] R. Bellman, Introduction to Matrix Analysis, Society for Industrial and Applied Mathematics, 1987.

[59] Quanser Inc., “SRV02 Rotary Pendulum User Manual,” 2010.

[60] J. Hespanha, Lecture Notes on LQR/LQG Controller Design, 2007.

[61] T. Takagi and M. Sugeno, “Fuzzy Identification of Systems and its Applications to Modeling and Control,” *Transactions on Systems, Man, and Cybernetics,* vol. 15, no. 1, pp. 116-132, 1985.

[62] K. Mehran, “Takagi-Sugeno Fuzzy Modeling for Process Control,” Newcastle University, 2008.

[63] H. Shousong and Z. Qixin, “Stochastic Optimal Control and Analysis of Stability of Networked Control Systems with Long Delay,” *Automatica,* vol. 39, no. 11, pp. 1877-1884, 2003.

[64] L. Montestruque and P. Antsaklis, “Stability of Model-Based Networked Control Systems with Time-Varying Transmission Times,” *IEEE Transactions on Automatic Control,* vol. 49, no. 9, pp. 1562-1572, 2004.

[65] M. Cloosterman, N. van den Wouw and W. Heemels, “Robust Stability of Networked Control Systems with Time-varying Network-induced Delays,” in *IEEE Conference on Decision and Control*, 2006.

[66] J. Nilsson, “Real-Time Control Systems with Delays,” PhD Thesis, Lund Institute of Technology, 1998.

[67] P. Albertos, A. Crespo, I. Ripoll, M. Valles and P. Balbastre, “RT Control Scheduling to Reduce Control Performance Degrading,” in *IEEE Conference on Decision and Control*, 2000.

[68] R. Chandra, X. Liu and L. Sha, “On the Scheduling of Flexible and Reliable Real-Time Control Systems,” *Real-Time Systems,* vol. 64, no. 2, pp. 153-169, 2003.

[69] G. Franklin, M. Workman and D. Powell, Digital Control of Dynamic Systems, Ellis-Kagle Press, 1997.

[70] J. Sandee, “Event-Driven Control in Theory and Practice,” PhD Thesis, Technische Universiteit Eindhoven, 2006.

[71] M. Guinaldo, D. Dimanagoras, K. Johansson, J. Sánchez and S. Dormido, “Distributed Event-Based Control for Interconnected Linear Systems,” in *IEEE Conference on Decision and Control and European Control Conference*, 2011.

[72] M. Guinaldo, D. Dimarogonas, K. Johansson, J. Sánchez and S. Dormido, “Distributed Event-Based Control Strategies for Interconnected Linear Systems,” *IET Control Theory & Applications,* vol. 7, no. 6, pp. 877-886, 2013.

[73] X. Chen and F. Hao, “Stability of Event-Triggered Output-Feedback Control Systems,” in *Chinese Control Conference*, 2011.

[74] J. VanAntwerp and R. Braatz, “A Tutorial on Linear and Bilinear Matrix Inequalities,” *Journal of Process Control,* vol. 10, no. 4, pp. 363-385, 2000.

[75] K. Gu, V. Kharitonov and J. Chen, Stability of Time-Delay Systems, Springer, 2003.

[76] B. Xu and Y. Liu, “An Improved Razumikhin-Type Theorem and Its Applications,” *Transactions on Automatic Control,* vol. 39, no. 4, pp. 839-841, 1994.

[77] X. Mao, “Comments on "An Improved Razumikhin-Type Theorem and Its Applications" [With Reply],” *Transactions on Automatic Control,* vol. 42, no. 3, pp. 429-430, 1997.

[78] F. Esquembre, “Easy Java Simulations: a Software Tool to Create Scientific Simulations in Java,” *Computer Physics Communications,* no. 156, pp. 199-204, 2004.

[79] F. Esquembre, “Easy Java Simulations,” [Online]. Available: http://fem.um.es/Ejs/.

[80] T. Shinbrot, C. Grebogi, J. Wisdom and J. Yorke, “Chaos in Double Pendulum,” *American Journal of Physics,* vol. 60, no. 6, pp. 491-499, 1992.

[81] E. Fridman, A. Seuret and J. Richard, “Robust Sampled-Data Stabilization for Linear Systems: an Input Delay Approach,” *Automatica,* vol. 40, no. 8, pp. 1441-1446, 2004.

[82] L. de la Torre and R. Heradio, “UNILabs,” Universidad Nacional de Educación a Distancia (UNED), [Online]. Available: http://unilabs.dia.uned.es/?lang=en.

APPENDICES

A. The SRV-02 motor model

On one hand, using Kirchhoff's second law in the circuit of Figure A.1 and that back-emf voltage (E_{emf}) is proportional to the speed of the motor shaft $\dot{\theta}_m$, it follows the electrical equations:

$$V_m(t) - R_m I_m(t) - L_m \frac{dI_m(t)}{dt} - k_m \dot{\theta}_m = 0.$$

Since $L_m \ll R_m$, the inductance (L_m) can be neglected and, solving for $I_m(t)$:

$$I_m(t) = \frac{V_m(t) - k_m \dot{\theta}_m}{R_m}.$$

On the other hand, from Newton's second law, the mechanical equations of the motor shaft are got:

$$J_m \ddot{\theta}_m = \tau_m - \frac{\tau_l}{\eta_g K_g} - B_m \dot{\theta}_m, \qquad (A.1)$$

where τ_m is the torque applied on the motor shaft, B_m the viscous friction acting on it and τ_l is the torque applied on the load.

Analogously, for the load of the motor:

$$J_l \ddot{\theta}_l = \tau_l - B_l \dot{\theta}_l, \qquad (A.2)$$

being B_l the viscous damping coefficient at load. Collecting the equations (A.1) and (A.2), it yields:

$$J_l \ddot{\theta}_l = \eta_g K_g \tau_m - \eta_g K_g J_m \ddot{\theta}_m - B_l \dot{\theta}_l - \eta_g K_g B_m \dot{\theta}_m. \qquad (A.3)$$

Since $\theta_m = K_g \theta_l$ and $\tau_m = \eta_m K_t I_m$, then (A.3) can be written finally as:

$$J_{eq} \ddot{\theta}_l = \eta_g K_g \eta_m K_t I_m - B_{eq} \dot{\theta}_l, \qquad (A.4)$$

where $J_{eq} = J_l + \eta_g K_g J_m K_g$ and $B_{eq} = B_l + \eta_g K_g^2 B_m$.

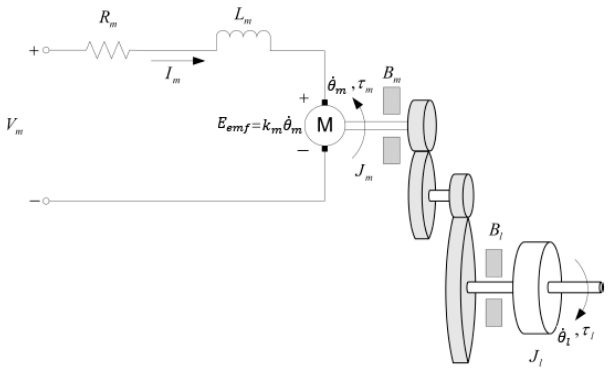

Figure A.1: Electrical circuit of the SRV-02 gear and gear train. Figure from Quanser Inc.

B. Razumikhin Theorem and Proposition 4.2 derivation

This appendix describes the Razumikhin theorem. It can be also found in the book of *Gu et al.* [75] with the corresponding proof.

Theorem B.1 (Razumikhin Theorem): Suppose $f: \mathbb{R} \times \mathcal{C} \to \mathbb{R}^n$ in a retarded system $\dot{x}(t) = f(t, x(t_k))$, takes $\mathbb{R} \times (bounded\ sets\ of\ \mathcal{C})$ into bounded sets of $\mathbb{R}^n$, and u, v, w are continuous nondecreasing functions, such that $u(x), v(x) > 0\ \forall x \neq 0$ and $u(0) = v(0) = 0$, v strictly increasing. If there exists a continuous functional $V: \mathbb{R} \times \mathbb{R}^n \to \mathbb{R}$ such that

$$u(\|x\|) \leq V(t, x(t)) \leq v(\|x\|), for\ t \in \mathbb{R}\ and\ x \in \mathbb{R}^n$$

and the derivative of V along the trajectories of the system satisfies:

$$\dot{V}(t, x(t)) \leq -w(\|x\|)\ whenever\ V\big(t + \theta, x(t + \theta)\big) \leq V(t, x(t))$$

for $\theta \in [-\delta, 0]$, then the system is uniformly stable.

If, in addition, $w(x) > 0$ for $x > 0$, and there exist a continuous nondecreasing function $q(x) > 0$ for $x > 0$ such that the above condition on $\dot{V}$ is reinforced:

$$\dot{V}(t, x(t)) \leq -w(\|x\|)\ whenever\ V\big(t + \theta, x(t + \theta)\big) \leq q\left(V\big(t, x(t)\big)\right)$$

for $\theta \in [-h, 0]$, then the system is asymptotically stable.

Next, using the following corollary of the Theorem B.1 and the improvement of the Razumikhin Theorem developed in [76], the Proposition 4.2 can be derived.

On one hand, we can formulate the corollary such that a time-delay system with maximum time-delay h is asymptotically stable if there exists a bounded quadratic Lyapunov function V such that for some $\varepsilon > 0$, it satisfies

$$V(x) \geq \varepsilon \|x\|^2$$

and its derivative along the system trajectory, $\dot{V}(x(t))$, satisfies

$$\dot{V}\big(x(t)\big) \leq -\varepsilon\|x\|^2$$

whenever

$$V\big(x(t+\xi)\big) \leq qV\big(x(t)\big), -h \leq \xi \leq 0$$

for some constant $q > 1$.

To prove this, it is only necessary to show that the Lyapunov function is such that $V(t, x(t)) \leq v(\|x\|)$, because the rest of the conditions of the Razumikhin theorem hold in the proposition. Since the Lyapunov function is bounded quadratic (For example $V = x^T(t)Px(t)$), then there always exists a sufficiently large constant C such that:

$$V \leq C\|x\|^2$$

Then for $v(\|x\|) = C\|x\|^2$, all the conditions of the Razumikhin theorem are satisfied.

On the other hand (see [76], [77]), less conservative conditions are obtained if all of the suppositions of the Razumikhin theorem are satisfied and $q_1 > 1$ is a constant. If there is a continuous function V such that:

i) For $t \in \mathbb{R}$ and $x \in \mathbb{R}^n$

$$u(\|x\|) \leq V(t, x(t)) \leq v(\|x\|);$$

ii) there is a $q_2 \geq 1/q_1$ such that

$$\sup_{\xi\in[-h,0]} V\big(t+\xi, x(t+\xi)\big) < q_1 V\big(t, x(t)\big)$$

at any $t \geq t_0$ implies

$$\sup_{\xi\in[-h,0]} \|x(t+\xi)\| \leq q_1 q_2 \|x(t)\| < u^{-1}\{q_1 v\|x(t)\|\}$$

at the same t;

iii) for any t_0

$$\dot{V}(t, x(t)) \leq -w(\|x\|) \; whenever \sup_{\xi \in [-h,0]} \|x(t+\xi)\| \leq q\|x(t)\|$$

for $\theta \in [-h, 0]$, then the system is asymptotically stable.

Finally, since a bounded quadratic Lyapunov function can satisfy the Razumikhin theorem in a restricted form, which is the necessary one to apply the less conservative condition $\|x(t+\xi)\| \leq q\|x(t)\|$, the Proposition 4.2 is obtained.